Boundary induced phase transitions in a traffic flow model with metastable states

Diplom-Arbeit im Fachbereich Physik

vorgelegt von

Alireza Namazi

aus Teheran / Iran

Referent: Priv. Doz. Dr. Andreas Schadschneider
Koreferent: Professor Dr. Ulrich Faigle

Mathematisch-Naturwissentschaftliche-Fakultät
Universität zu Köln

Köln, April 2001

Contents

Chapter 1

Introduction

For almost 50 years people have been trying to understand the problems of traffic flow using theoretical methods based on statistical physics [3, 4, 5, 6, 8, 10] and computer simulations. Until a few years ago most approaches were based on ”classical” methods from physics, especially from mechanics and hydrodynamics. Generally there are two different types of approaches: *microscopic* and *macroscopic* approaches.

There are several different types of mathematical formulations for the dynamical evolution of the system within the conceptual framework of microscopic approaches, in which single cars are modeled explicitly. The probabilistic description of vehicular traffic in the *kinetic theory* is developed by modifying the kinetic theory of gases. On the other hand, a deterministic description of the motion of individual vehicles is provided by *car-following theories* which are based on the basic principles of classical Newtonian dynamics. In contrast, the so-called *particle-hopping models* describe traffic in terms of stochastic movement of individual vehicles. For the latter the Asymmetric Exclusion Processes (ASEP) plays an important role for the understanding of system far from equilibrium. The one-dimensional ASEP is a lattice model describing particles hopping in one direction with hard core exclusion and stochastic dynamics first introduced in 1968 to provide a qualitative understanding of the kinetics of protein synthesis on RNA templates [27].

Computer simulations are helpful to get a deep insight into the various phenomena one finds in street traffic and to understand the basic principles that govern traffic systems. Moreover, since experiments with real traffic are infeasible, simulation models with high quantitative accuracy are necessary. Therefore, microscopic models of traffic have not only attracted the attention of a growing number of statistical physicists in recent years, but have also been received positively by many traffic engineers. Many mathematicians and computer scientists have recently interest in this field of research and use such models to find optimization strategies for transportation networks. The ongoing research efforts in the application of computer simulation in the frame of microscopic models for practical purposes in planning and design of transportation networks have been reviewed recently by Nagel et al. [9].

Some microscopic models are computationally quite efficient. For example cellular automaton (CA) models are discrete in space, time and state variables and for the simulations no differential equation has to be solved.

Krauss et al. [29, 30] introduced a whole class of stochastic models by considering necessary conditions for the collision-free motion of vehicles (SK). The models are continuous in space and discrete in time. The SK-model with periodical boundary conditions is well understood. In this work we study the behaviors of the SK-model with open boundary conditions and explore the structure of its phase diagram.

The models with open boundary conditions show different effects compared to their counterpart in periodic systems. One of the most fascinating effects observed for this models are so-called *boundary induced phase transitions*. This means the change of the bulk properties due to the variation of the boundary conditions. Recently a phenomenological theory was established, which is able to predict the phase diagram of open systems [7] in a general way.

Some relevant empirically observed features of real traffic are presented in chapter 2. Different model approaches are shortly described in chapter 3. The classification of the models into different classes is not unique.

The model introduced by Nagel and Schreckenberg (NaSch) [28] is a minimal CA model of traffic on highways; this model is presented in chapter 4. The SK-model that we investigate in this work is discussed in chapter 5. It can be seen as a further improvement of the CA model.

One of its most important features is the existence of metastable states and less is known on the behavior of such systems under open boundary conditions. The remaining chapters of this work deal with the properties of the SK-model with open boundaries. The difficulties in the definition of appropriate injection / extraction rules at the system borders are discussed in chapter 7. In chapter 8 and 9 the resulting phase diagram for two different injection rules are presented and results are compared to more general predictions about systems with open boundaries.

Chapter 2

Some empirical facts

In this section we present an overview of some of the empirical findings of vehicular traffic. The most important empirical result is the fact that a traffic flow can be found in three quite different states, namely free flow, jams and synchronized flow. These states could be identified in terms of a so-called *fundamental diagram*. Synchronized traffic is observed at high densities where interactions between cars are important. In spite of the drastically reduction of the average velocity, the flow by synchronized states can be close to the maximum value. This means that synchronized states are not dominated by jams but by cars moving close to each other with small velocities.

It is difficult to obtain reliable and reproducible detailed empirical data on vehicular traffic, in comparison with other fields of research in physical science. In vehicular traffic all empirical data have to be collected through passive observations, unlike controlled experiments used in many other fields of research in physics, providing the ability to make active experiments. Another problem is the dependence of traffic states on external influences like weather, which make it very difficult to have an unambiguous interpretation of these data.

2.1 The fundamental diagram

The traffic flow depends strongly on the occupancy of the road ρ.

One expects that the average speed $\langle v \rangle$ is practically independent of ρ so long as ρ is sufficiently small, because the vehicles are too far apart to interact with each other. Therefore, at sufficiently low density of vehicles, practically "free flow" takes place. It is seen in practical experiences that vehicles have to move slower with increasing density, one expects that at intermediate densities,

$$\frac{d\langle v \rangle}{d\rho} \leq 0, \tag{2.1}$$

when the forward movement of the vehicles is strongly hindered by others because of the reduction in the average separation between them (*gap*). This monotonic decrease of $\langle v \rangle$ with increasing ρ can lead to a maximum [12] in the current $\langle Q\rangle = \langle \rho v\rangle$ at $\rho = \rho_m$; for $\rho < \rho_m$, increasing ρ would lead to increasing $\langle Q\rangle$ whereas for $\rho > \rho_m$ sharp decrease of $\langle v\rangle$ with increase of ρ would lead to the overall decrease of $\langle Q\rangle$. In recent years some nontrivial variation of current with density have been observed. The nature of the variation of the current with the density is still not clearly understood [33].

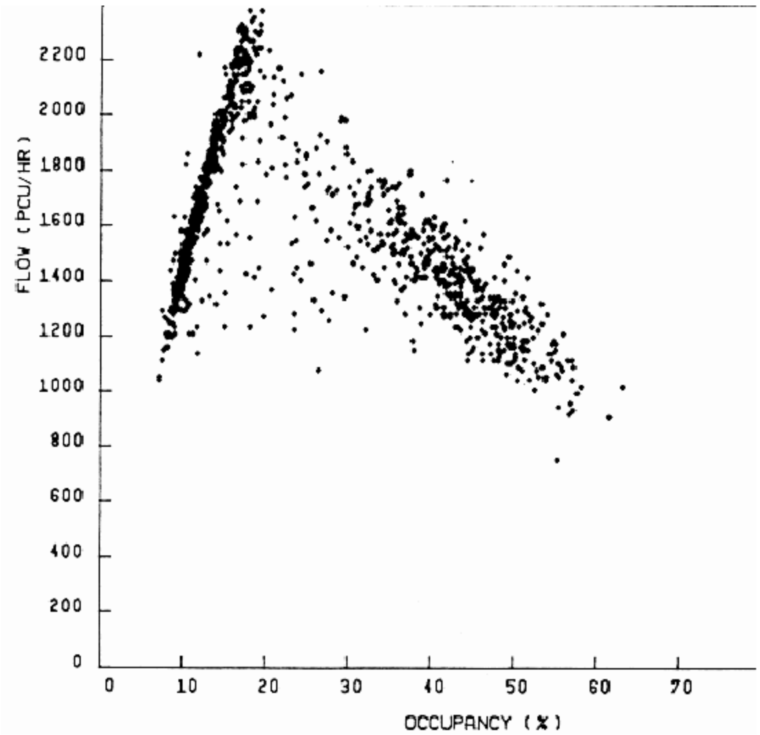

Figure 2.1: Empirical data for current and occupancy. The data have been collected by counting loops on a Canadian highway(from [33]).

Fig. 2.1 shows a typical time averaged local measurements of the density and current which have been obtained from the Queen Elizabeth Way in Ontario (Canada) [33]. At low densities there is a linear dependence of the current on the density. At high densities, increasing density causes decreasing in current.

In several situations it has been observed that the current Q does not depend uniquely on the global density ρ in an intermediate regime of density; it indicates the existence of *metastable stable stable and hysteresis effects*.

For such situations the fundamental diagram has two branches (Fig. 4.3) . This means, the same global density can either lead to a homogeneous state of high flow or to a state containing macroscopic jams. The point, where the branches intersect, corresponds to the point where the last jam dissolves, i.e. when the global density becomes equal to the density of the free flow ρ_1, which in equilibrium is equal to the density of the outflow from the jams. The upper branch is obviously metastable because any small jam would grow, so the system would be in jammed state (the lower branch).

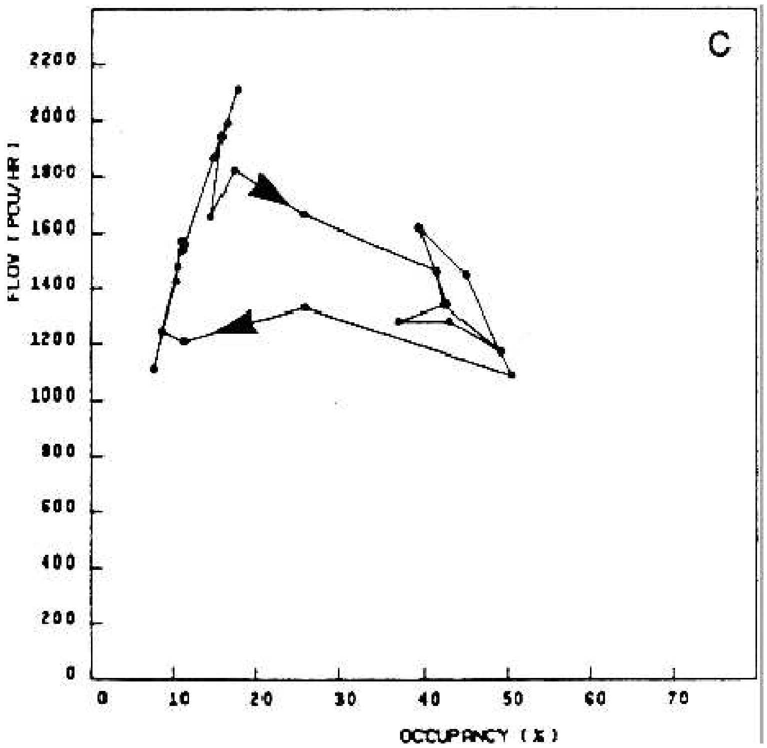

Figure 2.2: Time-traced measurements of the current (from [33]). Each data point corresponds to a time-averaged value of the current and density obtained from a local measurement. The average was performed over five minute intervals.

Hysteresis effects have the following meaning: if a measurement starts in the free flow regime, an increase of the density leads to an increase of the current. However, beyond a certain density, a further increase of the density leads to a *discontinuous* reduction of the stationary current ("capacity drop") and jams emerge. Decrease of the density does not recover the current.

Figure 2.2 shows an experimental verification of a hysteresis loop [33] at a transition from a free flow to a congested state.

2.2 Acceleration noise

Different drivers react differently to the same conditions on a highway, due to the different human temperaments and driving habits. Even on an empty stretch of a highway, when no other vehicle influences the motion of a vehicle, a driver would neither maintain a constant speed nor accelerate in a smooth fashion.

The *driver-to-driver fluctuation* of the acceleration depends on the density of vehicles on the highway and the type of the highway (i.e., the surface conditions, frequency of the curves, etc.). The distribution of the accelerations have been measured since mid nineteen fifties and are well documented [13, 35]. The root-mean-square deviation of the acceleration of the vehicles is a measure of the so-called *acceleration noise*.

2.3 Traffic jams

Traffic jams can emerge because of various different reasons. Traffic jams are often observed at bottlenecks, e.g. lane-reductions or crossings of highways [36]. At bottlenecks the capacity of the road is locally reduced thereby leading to the formation of jams. Traffic jams can be also emerge because of traffic accidents. It is very interesting that jams often appear, as if, from nowhere (apparently without obvious reasons) suddenly on crowded highways; these so-called "phantom jams" are formed by *spontaneous* fluctuations in an otherwise streamlined current.

Direct empirical evidence for this *spontaneous formation of jams* was presented by Treiterer [37] by analyzing a series of aerial photographs of a multi-lane highway. In Fig. 2.3 the picture from [37] is redrawn. Each line represents the trajectory of an individual vehicle on one lane of the highway[1]. The space-time plot ($x(t)$ diagram) shows the formation and propagation of a traffic jam. First time vehicles are well separated from each other. Then a dense region appears which, finally, leads to the formation of a jam. The jam remains stable for a certain period of time but, then, disappears again without any obvious reason. In this figure one can clearly see, that such jams can propagate upstream (opposite to the direction of flow of the vehicles). It also is possible that two or more jams coexist on a highway.

A more detailed analysis of traffic jams in absence of hindrances has been given by Kerner and Rehborn [38, 39, 40] who pointed out the following characteristic features of wide jams. They found that the upstream velocity and, therefore, the outflow from a jam is approximately constant. The outflow from a jam and the velocity of the jam fronts are now regarded as two important empirical parameters of highway traffic which can be used for calibrating theoretical models.

We can summarize the properties of traffic jams as following:

1. There are metastable states of high flow.
2. Traffic jams can develop and exist under "pure" conditions, i.e. in the absence of any obstacles.
3. The flux out of a jam is not maximal.
4. The outflow from jams is stable.
5. The outflow from jams and the velocity of the downstream front do not depend on the inflow conditions.

[1] The discontinuous trajectories correspond to vehicles changing the lane.

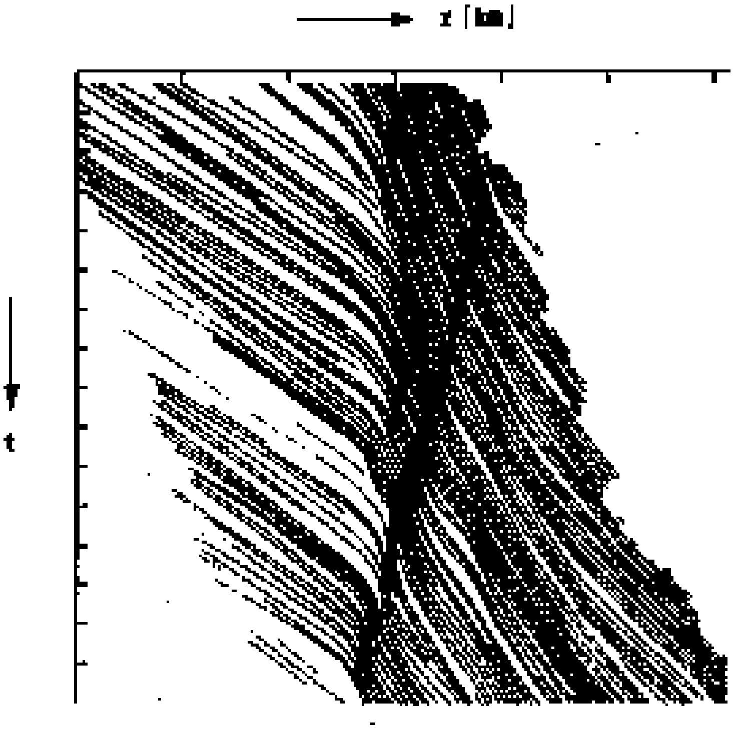

Figure 2.3: Trajectories of individual vehicles on a single lane of a multi-lane highway. The trajectories were drawn from aerial photographs. During the analyzed time-interval the spontaneous formation, propagation and dissolution of a jam has been observed (from [37]).

Chapter 3

Model approaches

Generally there are two different types of approaches: *microscopic* and *macroscopic* approaches. In "microscopic" models of vehicular traffic attention is explicitly focused on individual vehicles each of which is represented by a "particle"; the nature of the interactions among these particles is determined by the way the vehicles influence each others' movement. In other words, in the "microscopic" theories vehicular traffic is treated as a system of *interacting* "particles" *driven far from equilibrium* [24, 79, 25, 26]. In "macroscopic" models of vehicular traffic, traffic is viewed as a compressible fluid formed by the vehicles but these individual vehicles do not appear explicitly in the theory. In this section we present a brief overview of these model approaches.

3.1 Macroscopic models

Unlike microscopic models, in macroscopic approaches it is not the dynamics of individual vehicles that is considered, but the dynamics of quantities that only have a macroscopic meaning. In general, the vehicle density $\rho(x, t)$ and average velocity $v(x, t)$ are considered, which are both functions of space x and time t. These quantities are obtained by averaging over a region of sufficiently large spatial extent. Since the number of vehicles in a road segment can only change by vehicles entering or leaving the segment, an equation of continuity holds for ρ and v:

$$\frac{\partial \rho}{\partial t} + \frac{\partial}{\partial x}(\rho v) = 0 \, . \tag{3.1}$$

The model equations are closed assuming one more relationship between density and velocity. The simplest model of this kind was proposed by Lighthill and Whitham [56], where the velocity is assumed to be a function $V(\rho)$ of the density, leading to the model equation

$$\begin{aligned} \frac{\partial \rho}{\partial t} + c(\rho)\frac{\partial \rho}{\partial x} &= 0 \, , \\ \text{where} & \\ c(\rho) &= \frac{d}{d\rho}\left(\rho V(\rho)\right) \, . \end{aligned} \tag{3.2}$$

The model equation describes kinematic waves. The characteristics $x(\rho)$, i.e. the places where some prescribed density ρ is found, travel at the constant velocity $c(\rho)$. This model has been used very much in the last few decades. However, as pointed out by Kerner [43], it is not capable of describing the properties of clusters in traffic flow correctly. Nevertheless, still other models for kinematic waves have been proposed [57, 58, 59, 60, 61, 62].

The main problem about the Lighthill–Whitham approach is that it assumes local equilibrium. In general, one will have to replace the static relation $v(x, t) = V(\rho(x, t))$ by a dynamic equation that describes the way vehicles accelerate.

Payne formulated the dynamic equation for the velocity in the way that is in use today using the idea that the acceleration of a vehicle, which is the total time derivative of the velocity field $v(x, t)$, is described by a relaxation towards a local equilibrium velocity and an anticipation term, which can be identified with the pressure term in fluid dynamics. The idea that the pressure term describes anticipation is motivated by the fact that this term can be derived by assuming that a driver at point x adjusts to the conditions ahead at the point $x + 1/\rho$, where the preceding car is found. The resulting equation is

$$\frac{\partial v}{\partial t} + v\frac{\partial v}{\partial x} = \frac{V(\rho) - v}{\tau} - \frac{c_0^2}{\rho}\frac{\partial \rho}{\partial x} . \tag{3.3}$$

The left hand side of this equation is the total time derivative of the velocity, the first term on the right hand side describes relaxation, the second term anticipation. Unfortunately this model shows difficulties in the treatment of shock waves, because it develops solutions that are discontinuous in space. Different approaches were proposed to solve this problem [71, 64]. The most straightforward solution was given by Kühne, who introduced an additional viscous term that prevents the formation of discontinuities [20, 65, 69], the dynamical equation being

$$\frac{\partial v}{\partial t} + v\frac{\partial v}{\partial x} = \frac{V(\rho) - v}{\tau} - \frac{c_0^2}{\rho}\frac{\partial \rho}{\partial x} + \frac{1}{\rho}\frac{\partial}{\partial x}\left(\mu\frac{\partial v}{\partial x}\right) . \tag{3.4}$$

Kerner and Konhäuser [15, 76] used structurally the same model as Kühne, and investigated the nonlinear dynamics of cluster formation thoroughly. A recent work by Helbing [21] extends the Kerner–Konhäuser–theory by an equation for the velocity variance and takes into account that vehicles occupy a non-vanishing amount of space.

Similar models have also been formulated using discrete space coordinates right away [71, 72], leading to coupled ordinary differential equations or even coupled maps (if a forward discretization in time is used).

3.2 Microscopic models

Microscopic models of traffic flow describe the dynamics of each individual vehicle as a function of the positions and velocities of the neighboring vehicles. One can distinguish between car–following models and cellular automata models. In this section positions and velocities of all vehicles are denoted by x_i and v_i respectively, where the index i increases in downstream direction.

3.2.1 Car–following–Models

Deriving a car following theory can obviously always start from the quite reasonable assumption that a change of the velocity is only performed, if the momentary velocity does not coincide with some desired velocity V_{des}, which is determined by safety considerations, legal restrictions and so on. The simplest dynamics that describes how a driver tries to approach the desired velocity is that of a relaxation on some time scale τ:

$$\frac{dv_i(t)}{dt} = \frac{V_{\text{des}} - v_i}{\tau} \tag{3.5}$$

All car following theories can be traced back to this simple idea. Different models differ only in the choice of V_{des} and τ. Almost all car following theories are based on the assumption that the motion of vehicle i is governed exclusively by the motion of the preceding vehicle $i+1$. First of this model was introduced by Pipes [41]. In this model it is assumed that the desired velocity of a car is equal to the velocity of the car it is following, which would mean

$$\frac{dv_i(t)}{dt} = \frac{v_{i+1}(t) - v_i(t)}{\tau} \ . \tag{3.6}$$

This model is unable to describe clustering effects.

Bando et al. [14, 42] assumed that the desired velocity is a function of the distance between the vehicles under consideration:

$$\frac{dv_i(t)}{dt} = \left.\frac{V_{\text{des}}(x_{i+1} - x_i) - v_i}{\tau}\right|_t \ . \tag{3.7}$$

The function $V_{\text{des}}(\Delta x)$ has to vanish for $\Delta x \to 0$ and has to be bounded for $\Delta x \to \infty$. Bando et al. chose the desired velocity to be $V_{\text{des}}(\Delta x) = \tanh(\Delta x)$ and τ to be a constant. In this approach the speed–density–relation cannot be calculated from the model equations, but has to be prescribed through V_{des}.

This model is known as the *optimal velocity model*. It describes spontaneous clustering of vehicles (phantom jams). It has been shown on a phenomenological basis [43] that the qualitative dynamical properties of this model are almost exactly the same as those of the macroscopic Kerner–Konhäuser–Model [15, 76] and furthermore compare very well with empirical observations.

3.2.2 Coupled map modeling and cellular automaton

Instead of solving a differential equation for the velocities of the vehicles it is also possible to update the velocity in discrete time steps directly. The velocity of car i at time step t is calculated from the conditions ahead at time $t - \Delta t$:

$$v_i(t) = f(v_i(t - \Delta t), v_{i+1}(t - \Delta t), x_{i+1}(t - \Delta t) - x_i(t - \Delta t), \dots) \ . \tag{3.8}$$

The model of Yukawa et al is an example for such models [44, 16]. The model is deterministic, but the function f is chosen in such a way that the dynamics of the individual vehicles is chaotic.

Another example of this model type is the model proposed by Gipps [45], who started from considering braking distances of the vehicles and derived a safe (that means collision free) update scheme for the vehicle velocities from this. Under the assumption that drivers underestimate the braking capabilities of the car they are following, the Gipps–Model can describe over-reacting of drivers and correspondingly the existence of instabilities in traffic flow.

An even faster model is obtained, if the model is discretized not only with respect to time, but also with respect to the space coordinates. In this case a cellular automaton model of traffic flow is obtained and the whole dynamics can be simulated using only integer operations or even single bit coding. The first models of this kind were proposed by Cremer and Ludwig [17] and Schütt [46].

The most prominent representative of this class of models, however, is the Nagel–Schreckenberg–Model [18, 47, 48, 49, 50, 51]. This model will be discussed further in chapter 4.

The cellular automaton models are the first microscopic models that are computationally efficient enough to be used in large road networks, even for real–time applications.

Subsequently there have been efforts to build a bridge between cellular automata and space–continuous models and to perform other refinements to obtain quantitative agreement with empirical data [54, 55]. This will be explained in chapter 5.

Chapter 4

The Nagel–Schreckenberg–Model

The Nagel-Schreckenberg (NaSch) model [28] is a probabilistic cellular automaton (CA) able to reproduce the basic features of traffic flow as discussed in chapter 2. In a CA not only space and time are discrete, but also the state variable. In the NaSch model, each cell can be empty or occupied by exactly one car (Fig. 4.1). The state of the car is then characterized by its velocity v which can take one of the $v_{max} + 1$ allowed *integer* values $v = 0, 1, \ldots, v_{max}$. Suppose, x_n and v_n denote the position and velocity, respectively, of the n-th vehicle. Then, $d_n = x_{n+1} - x_n$, is the gap between the n-th car and the car in front of it at time t. At each time step $t \to t+1$, the arrangement of the N cars on a finite lattice of length L (i.e. for a global density $\rho = N/L$) is updated *in parallel* according to the following "rules":

Step 1: Acceleration.
If $v_n < v_{max}$, the speed of the n-th car is increased by one, i.e.

$$v_n \to \min(v_n + 1, v_{max}) \qquad \text{(U1).}$$

Step 2: Deceleration (due to other cars).
If $d_n \leq v_n$, the speed of the n-th car is reduced to $d_n - 1$, i.e.,

$$v_n \to \min(v_n, d_n - 1) \qquad \text{(U2).}$$

Step 3: Randomization.
If $v_n > 0$, the speed of the n-th car is decreased randomly by unity with probability p, i.e.,

$$v_n \to \max(v_n - 1, 0) \quad \text{with probability } p \qquad \text{(U3).}$$

Step 4: Car movement.
Each car is moved forward according to its new velocity determined in Steps 1–3, i.e.

$$x_n \to x_n + v_n \qquad \text{(U4).}$$

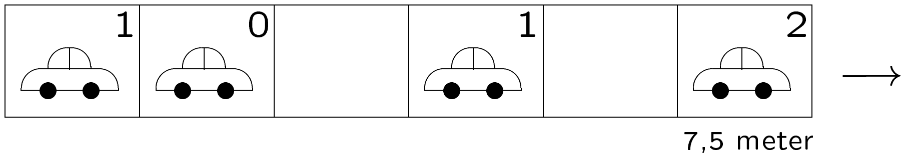

Figure 4.1: A typical configuration in the NaSch model. The number in the upper right corner is the speed of the vehicle (from [2]).

The NaSch model is a minimal model in the sense that all the four steps are necessary to reproduce the basic features of real traffic; however, additional rules are needed to capture more complex situations. Step 1 reflects the general tendency of the drivers to drive as fast as possible without crossing the maximum speed limit. Step 2 is intended to avoid collision between the cars. The randomization in step 3 takes into account the different behavioural patterns of the individual drivers, especially, nondeterministic acceleration as well as overreaction while slowing down; this is crucially important for the spontaneous formation of traffic jams. Even changing the precise order of the steps of the update rules stated above would change the properties of the model. E.g. after changing the order of steps 2 and 3 there will be no overreactions at braking and thus no spontaneous formation of jams (see below). The NaSch model may be regarded as stochastic CA [74].

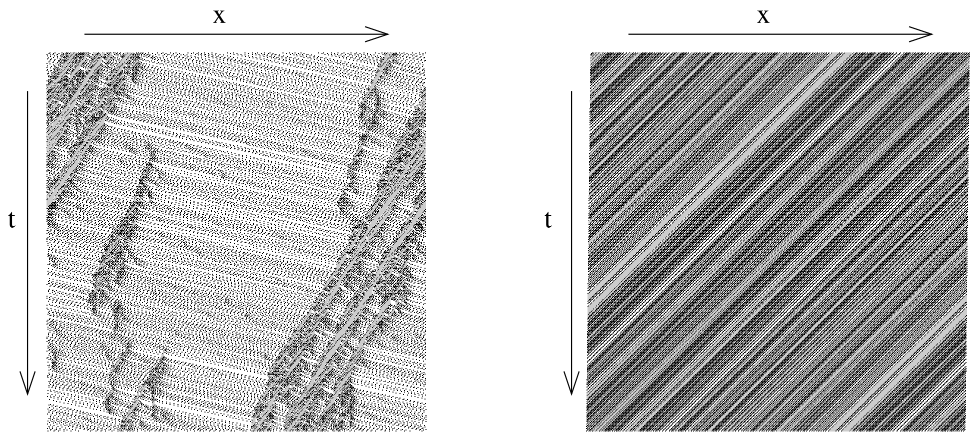

Figure 4.2: Typical space-time diagrams of the NaSch model with $v_{max} = 5$ and (a) $p = 0.25$, $\rho = 0.20$, (b) $p = 0$, $\rho = 0.5$ (from [2]).

Space-time diagrams showing the time evolutions of the NaSch model demonstrate that no jam is present at sufficiently low densities, but spontaneous fluctuations give rise to traffic jams at higher densities (Fig. 4.2(a)). From Fig. 4.2(b) it should be obvious that the *intrinsic stochasticity* of the dynamics, arising from non-zero p, is essential for triggering the jams. For a realistic description of highway traffic [28], the typical length of each cell should be about 7.5 m which is the space occupied by a car in a dense jam. When $v_{max} = 5$ each time step corresponds to approximately 1 sec of real time which is of the order of the shortest relevant timescale in real traffic, namely the reaction time of the drivers.

4.1 Generalizations and extensions of the NaSch model

4.1.1 Metastability, hysteresis and slow-to-start rules

As we saw in chapter 2, measurements on real traffic have revealed that traffic flow can exhibit metastability and hysteresis effects [40]. Fig. 4.3 shows a schematic fundamental diagram with a metastable branch. In the density interval $\rho_1 < \rho < \rho_2$ the flow is not uniquely determined but depends on the history of the system. Here a metastable high-flow branch exists. Metastable state is a homogeneous state of high flow in which each small jam would grow and cause the system have a jamming state. Closely related is the observation of hysteresis effects.

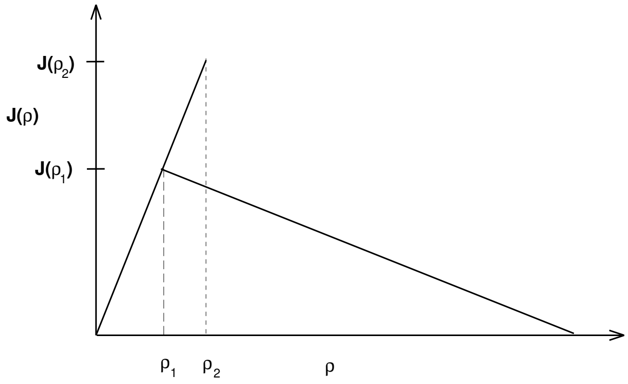

Figure 4.3: Schematic form of a fundamental diagram with metastable high-flow states (from [2]).

The NaSch model in its simplest form as introduced in chapter 4 does not exhibit metastable states and hysteresis. However, a simple generalization exists which is able to reproduce these effects. It is the so-called Velocity-Dependent-Randomization (VDR) model [75]. Here, in contrast to the original NaSch model, the randomization parameter depends on the velocity of the car, $p = p(v)$. The rules of chapter 4 are supplemented by a new rule,

Step 0: Determination of the randomization parameter. The randomization parameter used in step 3 for the n-th car is given by $p = p(v_n(t))$.

This new step has to be carried out before the acceleration step 1. The randomization parameter used in step 3 depends on the velocity $v_n(t)$ of the n–th car after the previous time step. Most relevant for an understanding of the occurrence of metastability and hysteresis are simple slow-to-start rules where one chooses [75]

$$p(v) = \begin{cases} p_0 & \text{for } v = 0, \\ p & \text{for } v > 0, \end{cases} \tag{4.1}$$

with $p_0 > p$. This means that cars which have been standing in the previous time step have a higher probability p_0 of braking in the randomization step than moving cars.

Fig. 4.4 shows a typical fundamental diagram obtained from computer simulations of the VDR model. It can be clearly seen that it has the same form as Fig. 4.3. Over a certain density interval $J(\rho)$ can take

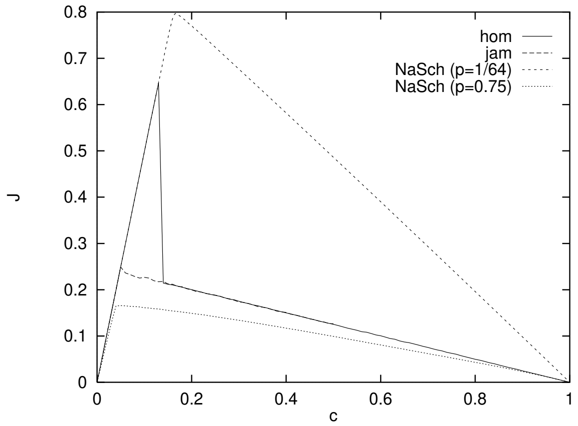

Figure 4.4: The fundamental diagram in the NaSch model with a velocity-dependent slow-to-start rule ($v_{max} = 5, p_0 = 0.75, p = 1/64$) obtained using two different initial conditions, namely, a completely jammed state (jam) and a homogeneous state (hom) (from [2]).

one of the two values depending on the initial state and, therefore, exhibit metastability. The microscopic structure of the states in the free-flow branch is very similar to that of the NaSch model. The metastable homogeneous states have a lifetime after which their decay leads to congested branch (see Fig. 4.5). In contrast, the microscopic structure of the congested branch differs drastically from the NaSch model. Here one observes phase separation into a macroscopic jam and a macroscopic free-flow regime (see Fig. 4.5).

It is instructive to compare the fundamental diagram of the VDR model with those of the corresponding NaSch models. The fundamental diagram of the VDR model can be understood from heuristic arguments utilizing the observed structures of the steady-states. For small densities $\rho \ll 1$ there are no slow cars in the VDR model since interactions between cars are extremely rare. Every car moves with the free-flow velocity $v_f = v_{max} - p$ and, therefore, the flux is given by

$$J_{hom}(\rho) = \rho(v_{max} - p) \tag{4.2}$$

which is identical to the NaSch model with randomization p. On the other hand, for densities close to $\rho = 1$, the cars are likely to have velocities $v = 0$ or $v = 1$ only and, therefore, the random braking is dominated by p_0. A simple waiting time argument [75] shows that the flow in the phase-separated regime is given by

$$J_{sep}(\rho) = (1 - p_0)(1 - \rho). \tag{4.3}$$

This corresponds to the NaSch model with randomization p_0 (see Fig. 4.4).

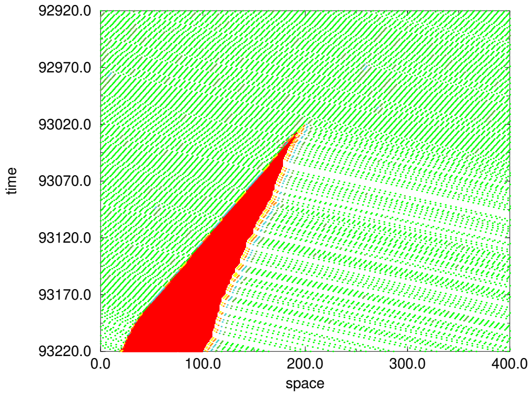

Figure 4.5: Typical space-time diagram of the VDR model with $v_{max} = 5$ and $\rho = 0.20$, $p = 0.01$ and $p_0 = 0.75$. Each horizontal row of dots represents the instantaneous positions of the cars moving towards right while the successive rows of dots represent the positions of the same cars at the successive time steps (from [2]).

The behaviour found in the VDR model is generic for models with slow-to-start rules. Due to the slow-to-start rule the outflow from a large jam is smaller than the maximal possible flow, i.e. the maximum of the fundamental diagram. Therefore the density far downstream is rather small and the vehicles propagate almost freely in the low-density region. The spontaneous formation of jams is suppressed if p is not too large. This is the basic mechanism which leads to the formation of the phase-separated state and hysteresis.

Chapter 5

SK-model

Stefan Krauss introduced an extension of the Nagel-Schreckenberg-Model which is known as *SK-model* [1],[30]. In SK-model, unlike Nagel-Schreckenberg-Model the state variables, i.e. space and velocity are chosen to be continuous. There is also a maximum acceleration and deceleration rates introduced, which causes the model having metastable states. To make the model safe (free of crashes), SK-model introduce a safe velocity v_{safe} for each car, which would be calculated in each time step. The vehicles will be updated parallel an a periodic boundary conditions is used.

Krauss proposed a family of stochastic microscopic traffic flow models , that has been derived from quite general and simple assumptions about traffic. Depending on how the free parameters characterizing acceleration and deceleration capabilities are chosen, three qualitatively different classes of models are obtained (see Fig. 5.1). The model classes can be characterized by referring to the properties mentioned in section 2.3 as follows:

- Class *I*:
  - Accelerations and decelerations realistic and bounded, i.e. long ranged interactions.
  - All properties of jams are modeled correctly.
  - The jamming transition is a first order phase transition.
- Class *II*:
  - Decelerations are unbounded, i.e. short ranged interactions.
  - Properties *i*,*iii*, and *iv* of jams are not reproduced.
  - The jamming transition is no phase transition.
- Class *III*:
  - Accelerations are unbounded.
  - No jams exist.

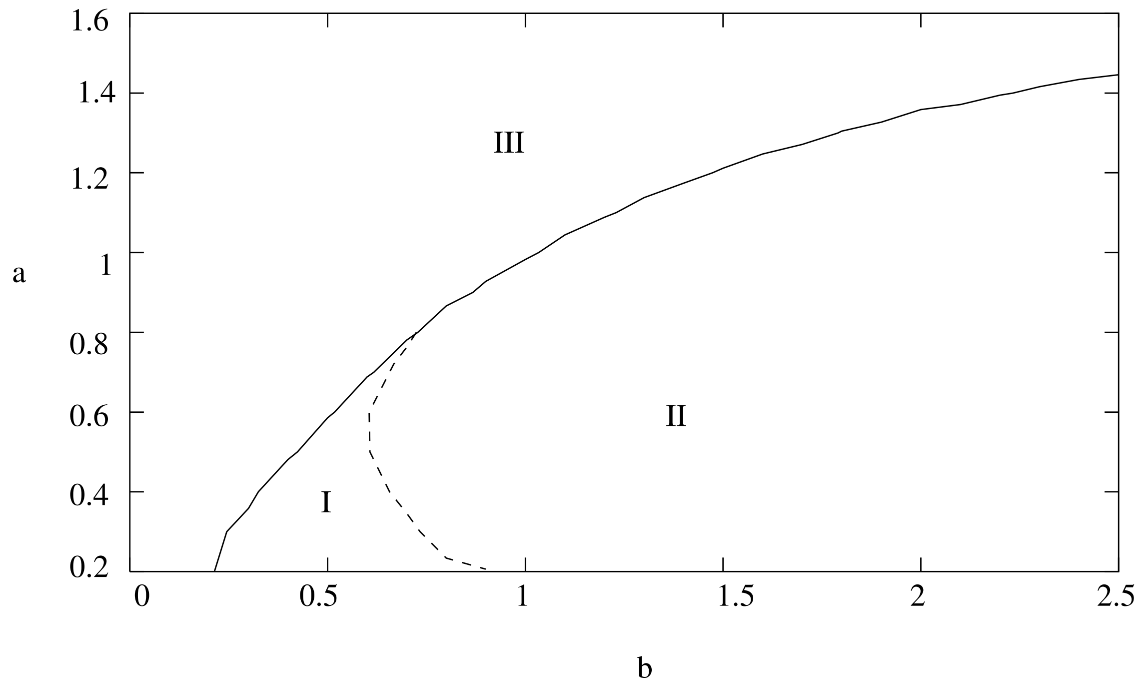

Figure 5.1: Model classes. In class *I* accelerations and decelerations are realistic and all properties of jams are modeled correctly. In class *II* decelerations are unbounded and the properties *i*,*iii*, and *iv* of jams are not reproduced. In class *III* accelerations are unbounded and no jams exist (from [1]).

From a phenomenological point of view also other models can be attributed to these classes. Phenomenologically the macroscopic Kerner–Konhäuser–Model [76], the microscopic Bando–Model [14], and some cellular automaton models using so called "slow–to–start–rules" [77, 23], that have recently been developed, are all models of class *I*, too. The Nagel–Schreckenberg–Model [48], which is a model of class *II*, apart from the discreteness of the space coordinate. The stochastic version of the Fukui–Ishibashi model [78] is a model of class *III*.

To extract the model equations two types of motion of vehicles are considered. The first type is the free motion of a vehicle, the second is the motion of a vehicle while interaction with another vehicle takes place. Corresponding to this, two main assumptions can be made. The main property of free motion is, that the velocity at which a vehicle moves is bounded by some maximum velocity v_{max}:

$$v \leq v_{\mathrm{max}} \ . \tag{5.1}$$

The maximum velocity can be interpreted as the desired velocity of the driver under consideration.

The reason why vehicles interact at all, is the fact, that drivers have the intention not to collide with any other car. So the second assumption Krauss made was, no matter how interaction actually takes place on the level of perception and decision making, it always turns out in such a way that the system remains free of collisions. So he assumed that a driver always chooses a velocity that is no higher than the maximum safe velocity v_{safe}:

$$v \leq v_{\text{safe}} \ . \tag{5.2}$$

The way the maximum safe velocity is determined specifies the way vehicles interact and will be considered in the next subsection.

Furthermore it is assumed that positive and negative accelerations are bounded:

$$\begin{aligned} -b \leq \tfrac{dv}{dt} \leq a \ , \\ a, b > 0. \end{aligned} \tag{5.3}$$

it is assumed that the updates are in discrete time steps Δt . The above restrictions can be formulated as:

$$v(t + \Delta t) \leq \min[v_{\max}, v(t) + a\Delta t, v_{\text{safe}}] \ , \tag{5.4}$$

where v_{safe} is calculated under the restriction

$$v(t + \Delta t) \geq v(t) - b\Delta t \ . \tag{5.5}$$

The complete information about how the individual vehicles interact is contained in the way v_{safe} is calculated. Once v_{safe} is determined, inequality (5.4) constitutes an update scheme for a traffic flow model, if the velocities of the vehicles are always chosen to be the highest velocities compatible with the above restrictions.

5.1 Modeling of interactions

5.1.1 Time continuous description

To complete the traffic flow model, the interactions have to be modeled. We look at a pair of cars, a leader at position x_{l} with velocity v_{l} and a follower at position x_{f} with velocity v_{f}. If the vehicle length is l, the gap g between the vehicles is given by

$$g = x_{\text{l}} - x_{\text{f}} - l \ . \tag{5.6}$$

As mentioned before, the reason for interaction is the intention of drivers to move without colliding with any other car. That means the gap g always has to be nonnegative.

Krauss showed that in a time continuous model interacting vehicles certainly do not collide if the gap g between the leading and the following vehicle is larger than some nonnegative desired gap g_{des} once and obeys the dynamical inequality

$$\frac{dg}{dt} \geq \frac{g_{\text{des}} - g}{\tau_{\text{des}}} \ . \tag{5.7}$$

The desired relaxation time τ_{des} and the desired gap g_{des} may be functions of the gap between the vehicles and their velocities. The fact that collisions cannot occur in this model is obvious, because for $g = 0$ the time derivative of g is always nonnegative if g_{des} is.

Consider the case of a leader and a follower with a gap g between them at velocities v_{l} and v_{f}, respectively. The follower travels at a safe velocity, if the driver can, under any circumstances, bring the car to a complete stop before colliding with the preceding vehicle. That means, if the follower has a reaction time τ and the braking distance of the vehicles from velocity v is given by the function *brake*(v), the situation is safe, if

$$d(v_{\text{f}}) + v_{\text{f}}\tau \le d(v_{\text{l}}) + g \ . \tag{5.8}$$

Inverting this inequality with respect to v_{f} would lead to a safe update rule for the velocity of the follower. To solve the inequality , Krauss performed a Taylor series expansion of the braking distance *brake*(v) around the average velocity of the leader and the follower $\bar{v} = (v_{\text{l}} + v_{\text{f}})/2$. Obviously the even orders of the series cancel out from the inequality and dropping only the third and higher order terms and we get:

$$brake'(\bar{v})v_{\text{f}} + \tau v_{\text{f}} \le brake'(\bar{v})v_{\text{l}} + g. \tag{5.9}$$

An interpretation of the derivative *brake*$'(v)$ can be given easily. Looking at a car decelerating from velocity v to velocity 0 at some (not necessarily constant) rate $\dot{v} = -b(v)$, $b(v) > 0$ it can be seen that:

$$\begin{aligned} brake'(v) &= -\frac{d}{dv}\int_v^0 \frac{v'}{b(v')}dv' \\ &= \frac{v}{b(v)} \ . \end{aligned} \tag{5.10}$$

Now the safety condition can be restated as:

$$v_{\text{l}} - v_{\text{f}} \ge \frac{v_{\text{l}}\tau - g}{\frac{\bar{v}}{b(\bar{v})} + \tau} \ . \tag{5.11}$$

Note that:

$$\frac{dg}{dt} = v_{\text{l}} - v_{\text{f}}. \tag{5.12}$$

So inequality (5.11) takes exactly the form of inequality (5.7) with the desired gap $g_{\text{des}} = v_l\tau$ and desired relaxation time $\tau_{\text{des}} = \tau_{\text{b}} + \tau$, where $\tau_{\text{b}} = \bar{v}/b(\bar{v})$ is determined by the typical decelerations b that a driver is willing to use. Note that by deriving inequality (5.11) considering non-vanishing braking distances, the effect of negative accelerations being bounded by $-b$ has been incorporated.

5.1.2 Discrete time steps

The inequalities derived so far have to be modified slightly to provide a scheme for updates of the vehicles' velocities in discrete time steps. The use of discrete time steps also provides a crude model for effects of finite reaction time.

The most natural way to construct an update scheme from the safety condition is to interpret the velocity v_f in the expression for $\dot{g}(t) = v_l(t) - v_f(t)$ as the velocity of time step $t + \Delta t$ leading to

$$v_f(t + \Delta t) \leq v_l(t) + \frac{g(t) - g_{des}(t)}{\tau_{des}(t)} \ . \tag{5.13}$$

The space coordinate x of the cars will be updated according to

$$x(t + \Delta t) = x(t) + v(t + \Delta t)\Delta t \ . \tag{5.14}$$

We know that for $\Delta t \rightarrow 0$ and $g_{des} \geq 0$ this rule guarantees safety. For finite Δt safety has to be checked again, however.

Having a gap $g(t)$ between a pair of vehicles at time t, the gap at time $t + \Delta t$ is given by

$$g(t + \Delta t) = g(t) + \Delta t \left(v_l\left(t + \Delta t\right) - v_f\left(t + \Delta t\right)\right) \ . \tag{5.15}$$

Inserting inequality (5.13) yields:

$$\begin{aligned} \xi(t + \Delta t) &\geq \xi(t)\left(1 - \tfrac{\Delta t}{\tau_b + \tau}\right) + \Delta t \ \tfrac{g_{des}(t) - v_l(t)\Delta t}{\tau_b + \tau} \ , \\ &\text{where} \\ \xi(t) &= g(t) - v_l(t)\Delta t \ . \end{aligned} \tag{5.16}$$

So safety ($g \geq 0$) is guaranteed, if $\xi(t = 0) \geq 0$ and

$$\begin{aligned} \Delta t &\leq \tau \\ &\text{and} \\ g_{des} &\geq v_l \Delta t \end{aligned} \tag{5.17}$$

for $t > 0$. This, of course, is exactly the result that had to be expected. It only states that the update rule is safe, if the true reaction time (i.e. the length of one time step) is smaller than or equal to the reaction time that each driver assumes, when choosing a driving strategy.

5.2 The model equations

It will be assumed that, apart from random fluctuations, every vehicle moves at the highest velocity compatible with the restrictions stated above. In this way the model can be formulated immediately, giving

$$\begin{aligned} v_{safe}(t) &= v_l(t) + \tfrac{g(t) - g_{des}(t)}{\tau_b + \tau} \ , \\ v_{des}(t) &= \min[v_{max}, v(t) + a(v)\Delta t, v_{safe}(t)] \ , \\ v(t + \Delta t) &= \max[0, v_{des}(t) - \eta] \ , \\ x(t + \Delta t) &= x(t) + v\Delta t \ . \end{aligned} \tag{5.18}$$

The desired gap g_{des} can be chosen in different ways. In SK-model the desired gap is chosen to be $g_{\mathrm{des}} = \tau v_{\mathrm{l}}$ and τ is the reaction time of the drivers. The time scale τ_{b} is defined as $\tau_{\mathrm{b}} = \bar{v}/b$. Here the random perturbation $\eta > 0$ has been introduced to allow for deviations from optimal driving.

We can rewrite this briefly as:

$$\begin{aligned} v_{\mathrm{des}} &\leftarrow min[v_{\max}, v + a, v_{\mathrm{safe}}] \;, \\ v &\leftarrow max[0, rand[v_{\mathrm{des}} - \epsilon a, v_{\mathrm{des}}]] \;, \\ x &\leftarrow x + v, \end{aligned} \tag{5.19}$$

where $rand[x_1, x_2]$ denotes a random number between x_1 and x_2.

5.3 Characteristics of the model

The SK-model characteristics should be also reproduced in systems with open boundary conditions, which are described in the following sections. In this section we would like to show some of the most important characteristics of the SK-model.

The SK-model shows metastable states of high flow, which can be seen in the fundamental diagram. Fig. 5.2 shows a fundamental diagram for a system with the following parameters: $a = 0.1$, $b = 0.6$, $v_{max} = 5$, $\epsilon = 1.0$, $l_{car} = 1.0$.

For densities $0.1 \leq \rho \leq 0.14$ we state *metastable states* of high flow.

The distribution of *gap*s and velocities of a system in jammed state has two peaks, which means that there are two groups of cars in the system. The first group has a high velocity and there is a big *gap* between these cars. The second group are the cars with low velocities moving close to each other (see Figs. 5.3 , 5.4).

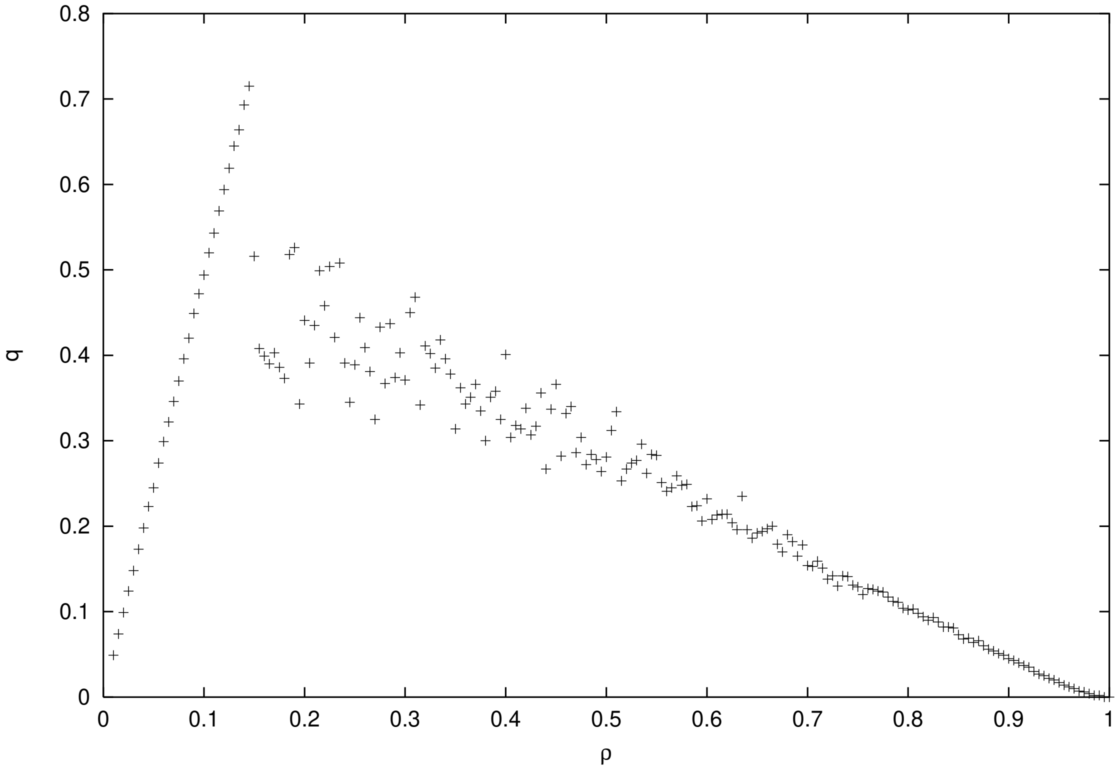

Figure 5.2: Fundamental diagram of the SK-model with periodical boundary conditions. The density is a mean value of densities measured in an interval of $\frac{L_{system}}{3}$ located in the middle of the system. The *current* was measured locally in the middle of the system. For densities $0.1 \leq \rho \leq 0.14$ we find *metastable states* of high flow.

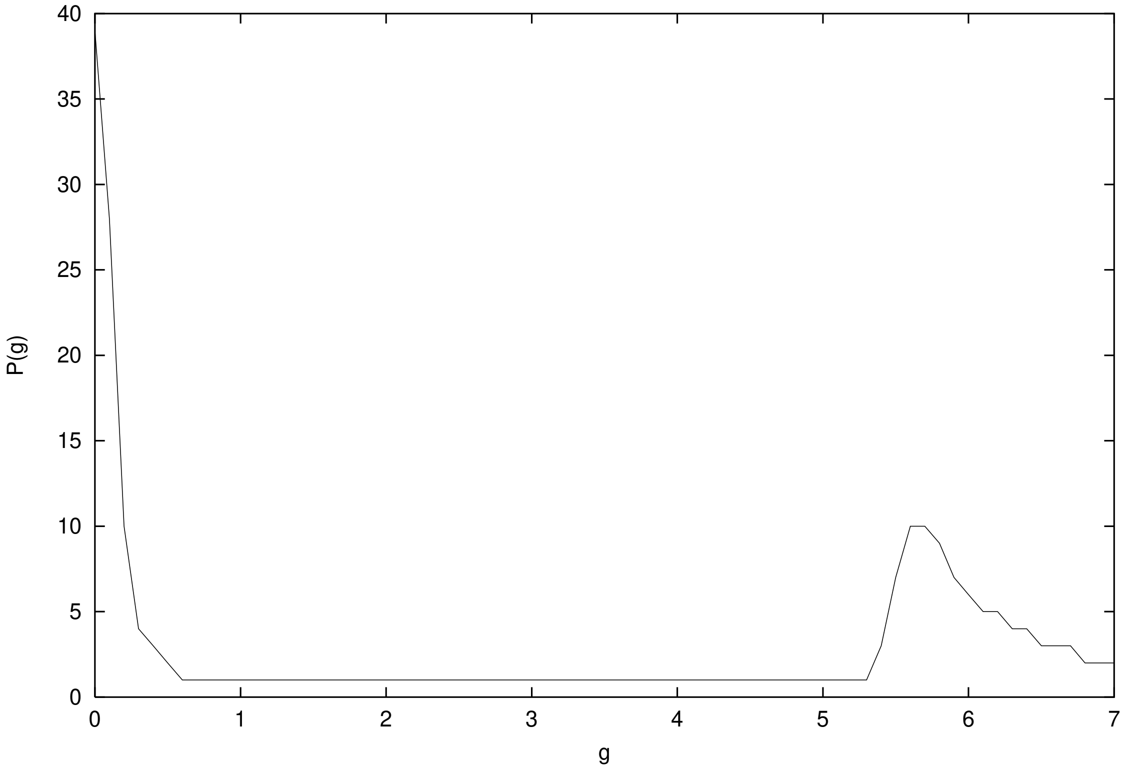

Figure 5.3: Distribution of *gap*s for the SK-model with periodical boundary conditions in jammed state. The distribution of *gap*s has two peaks, which means that there are two groups of cars in the system. The cars in the first group are moving far from each other (the *gap* between these cars is big), the second group are cars traveling close to each other.

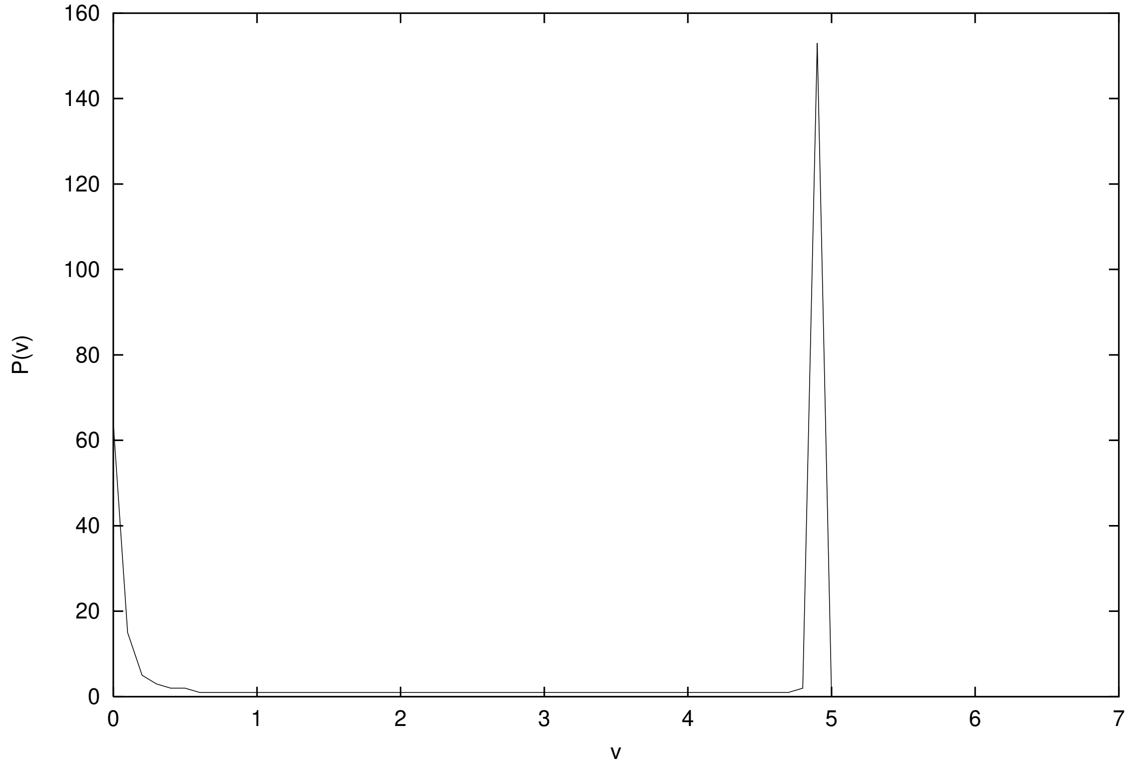

Figure 5.4: Distribution of *velocities* for the SK-model with periodical boundary conditions in jammed state. The distribution of velocities has two peaks, which means that there are two groups of cars in the system. The first group have high velocities, the second group are cars with low velocities.

Chapter 6

Open boundary conditions

6.1 Introduction

One of the most significant differences between systems with open and periodic boundary conditions is the car density ρ, which in a periodic system is a tuning parameter. The probability to find a car within an interval Δx is $\frac{\rho \Delta x}{l_{car}}$. In systems with periodical boundary conditions, for a given density ρ, it is easy to find a homogeneous initial configuration, which makes it possible to control some of the system behaviors. For example, in the SK-Model, the system will remain free of crashes, if the system has an initial configuration, which gives us a crash free system at $t = 0$. On the other hand, in systems with open boundary conditions, the situation is totally different. In these systems one has to deal with two different tuning parameters, namely the injection rate α and the extraction rate β . One tries to inject cars with probability of α. The cars will leave the system with probability of β. This means that the car density in the bulk will be a derived parameter.
The influence of α and β on the car density implies that quantities like global density, current, and the density profiles, show a different behavior than in periodic systems , which were studied for the asymmetric simple exclusion process (ASEP) [66], [67] - [68].

The asymmetric simple exclusion process is the simplest prototype-model of interacting systems driven far from equilibrium. It is a generic model for studying driven systems and boundary induced phase transitions. [24, 79], [68]. In the following section(6.2) a brief overview of the ASEP is presented.

For deriven lattice systems which exhibit metastable states in periodic systems is still less known, although they are relevant in different fields. In section (6.3) we present an overview of a recent study done by Appert and Santen [22], analyzing a driven lattice gas exhibiting metastable states.

6.2 ASEP with open boundary conditions

The ASEP (Fig. 6.1) is a discrete particle hopping model, a particle can move forward one cell with probability p if the lattice site immediately in front of it is empty. If the first cell is empty a particle will be injected there with probability α. If the last cell is occupied the particle will be removed with probability β.

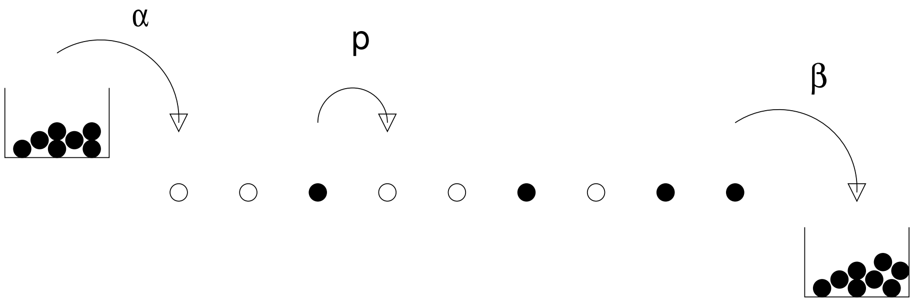

Figure 6.1: The asymmetric simple exclusion process (from [2]).

By varying the tuning parameters α and β and therefore the densities of the boundaries, one obtains a surprisingly rich phase diagram (see Fig. 6.5) .

One distinguishes between three different phases, examining the functional dependence of the current through the system on the system parameters. In the low-density phase A ($\alpha < \beta, \alpha_c(p)$) the current is independent of β. Here the current is limited by the rate α which then dominates the behavior of the system. In the high-density phase B ($\beta < \alpha, \beta_c(p)$) the behavior is dominated by the output rate β and the current is independent of α. In the maximum current phase C ($\alpha > \alpha_c(p)$ and $\beta > \beta_c(p)$) the limiting factor for the current is the bulk rate $q = 1 - p$. Here the current becomes independent of both α and β.

The transitions between the phases can be characterized by the behavior of two correlation lengths ξ_α and ξ_β . These are the length scales on which the density at the system boundaries depends. Apart from ξ_α and ξ_β also a third length $\xi^{-1} = |\xi_\alpha^{-1} - \xi_\beta^{-1}|$ plays an important role.

The transition from A (B) to C is continuous with diverging correlation length ξ_α (ξ_β). The transition from the high- to the low-density phase is of first order. Here both ξ_α and ξ_β are finite, but ξ diverges. On the transition line one finds a linear density profile created by the diffusion of a domain wall between a low-density region at the left end of the chain and a high-density region at the right end.

In [7] a nice physical picture has been developed which explains the structure of the phase diagram not only qualitatively, but also quantitatively. With considering the collective velocity

$$v_c = j'(\rho) \tag{6.1}$$

which is the velocity of the center of mass of a local perturbation in a homogeneous, stationary back-

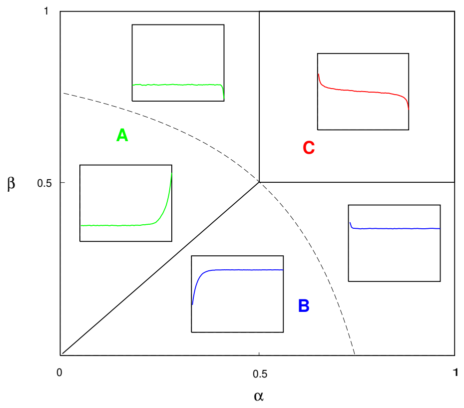

Figure 6.2: Phase diagram of the ASEP. The inserts show the typical form of the density profiles. In the low-density phase A the current is independent of β. Here the current is limited by the rate α, which then dominates the behavior of the system. In the high-density phase B the behavior is dominated by the output rate β and the current is independent of α. In the maximum current phase C the limiting factor for the current is the bulk rate $q = 1 - p$. Here the current becomes independent of both α and β (from [2]).

ground of density ρ (Fig. 15(a)) and the shock velocity

$$v_s = \frac{j_2 - j_1}{\rho_2 - \rho_1} \tag{6.2}$$

of a 'domain wall' between two stationary regions of densities $\rho_{1,2}$ (Fig. 15(b)), one can understand the phase diagram of systems , with a single maximum in the fundamental diagram [83],[7] An example is given in this work. More detailed discussion can be find in [83]. Notice that both velocities may change sign, depending on the densities at the boundaries.

In general one finds [83],[7] that the current always obeys an extremal-principle (extremal-current principle)

$$j = \max_{\rho\in[\rho^+,\rho^-]} j(\rho) \text{ for } \rho^- > \rho^+ \tag{6.3}$$

$$j = \min_{\rho\in[\rho^-,\rho^+]} j(\rho) \text{ for } \rho^- < \rho^+. \tag{6.4}$$

ρ^- and ρ^+ are the left and right boundary densities respectively.

For example we consider a situation with low ρ^- slightly below ρ^+ with just a single shock separating both regions. According to (6.2) the shock travels with speed $v_s = (j^+ - j^-)/(\rho^+ - \rho^-) > 0$ to the right, making the bulk density equal to ρ^-. At the same time, small disturbances will according to (6.1) also drift to the right, as $v_c = j'(\rho^-) > 0$ in this region, thus stabilizing the single shock. According to (6.4) the current will be the point in the fundamental diagram of the periodic system with $\rho = \rho^+$.

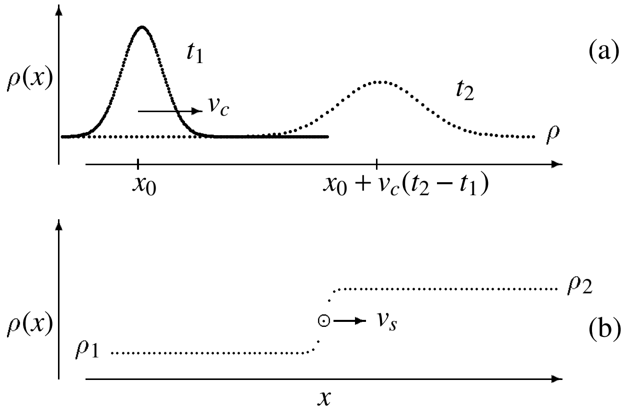

Figure 6.3: (a) Diffusive spreading of a density perturbation in the stationary state at two times $t_2 > t_1$. The collective velocity describes the motion of the center of mass of the perturbation. (b) Motion of a shock. To the left of the domain wall particles are distributed homogeneously with an average density ρ_1. To the right of the domain wall the background density is ρ_2 (from [83]).

So the phase diagram of the open system will be completely determined by the fundamental diagram of the periodic system through the extremal-current principle and therefore independent of the microscopic dynamics of the model.

6.3 Driven lattice gases with metastable states

In this section, we present a study of a driven lattice gas model which shows metastable on a periodic lattice, done by Appert and Santen [22]. First we discuss briefly the case of perodical boundary conditions.

The deriven lattice gas model is defined on a chain of length L. Each site of the chain may either be empty or occupied with a particle of velocity zero (0) or one (1). In a first step all particles which moved in the previous time step keep their velocity *if* the next site is empty. With probability q_0, velocity one is assigned to particles with velocity zero and an empty site ahead. In all other cases velocity zero is assigned to the particle. In the second step particles with velocity one move to the next site. Both steps are applied synchronously to all particles.

This model may be interpreted as a special case of the *VDR* model for traffic flow introduced in section 4.1.1, i.e. we restrict the maximal velocity of the particles to one.

The structure of the fundamental diagram, in the case of periodic boundary conditions is a key to understand the behavior of the open chain (see section 6.2). Fig. 6.4 shows the numerically established fundamental diagram for this model.

The form of the fundamental diagram can be easily understood in comparison with:

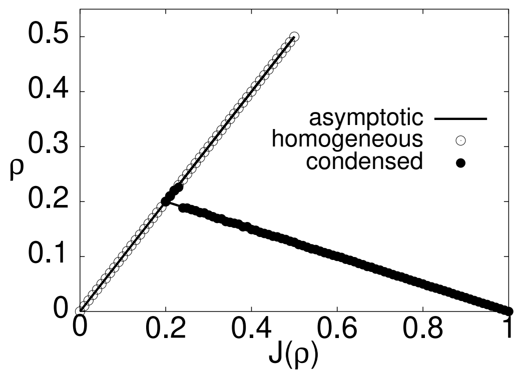

Figure 6.4: The fundamental diagram for periodical boundary conditions with $q_0 = 0.25$ and $L = 1,000$. Empty circles show simulation results for an initialization where all particles have velocity one and at least one empty site in front. Filled circles show results starting the simulation with a compact cluster of particles. These results are compared to the estimate for $L \to \infty$ (solid line). (From [22])

$$\begin{aligned} J(\rho) &= \rho \quad \text{if } 0 \le \rho \le 0.5 \\ J(\rho) &= q_0(1-\rho) \quad \text{if } q_0/(1+q_0) \le \rho \le 1 \end{aligned}$$

For densities $0 \le \rho \le 0.5$ and suitable initial configurations (the initial velocity of the particles is one and no particle is blocked) all particles move deterministically with velocity one. At larger densities $\rho > 0.5$ the number of particles exceeds the number of holes, i.e. one cannot avoid the formation of clusters of particles. The simulation results indicate that in the steady state one observes phase separation, i.e. the formation of a large compact cluster of particles which coexists with a free-flow regime. The density in the free-flow regime is determined by the frequency of particles leaving the cluster. The typical time the first particle needs to separate from the cluster is simply given by $T = q_0^{-1}$. This time already determines the average gap between two particles in the low-density regime. Therefore the average density, ρ_{free} in the free-flow regime is given by $\rho_{free} = 1/(T+1) = q_0/(1+q_0)$. The number of moving particles and therefore the flux follows from particle conservation.

Both solutions for $J(\rho)$ coexist for $\rho_{free} \le \rho \le 1/2$. For finite systems it is possible that the large cluster dissolves due to fluctuations. In free flow states, fluctuations are absent and therefore no spontaneous cluster formation takes place at densities $\rho \le 0.5$. However, in the thermodynamic limit, any random initial configuration leads to a jammed stationary state.

Now we consider the open chain. Open boundary conditions are implemented as follows : at the left boundary particles with velocity one are introduced with probability α if the first site of the chain is empty. At the right end the particles leave the chain from site L with probability β, irrespective of their velocity.

The values of α and β determine for given values of L and q_0 the bulk behavior of the system. First we notice that for $\beta = 1$ the only stochastic element is due to the left boundary, i.e. we recover the deterministic asymmetric exclusion process. Therefore the exact result for the flow is given by $J(\alpha) = \alpha/(1+\alpha)$. This result for the flow is expected to be valid not only for $\beta = 1$ but in the whole low density phase, because for low bulk densities the flow is controlled by the input of particles.

Next, we consider the case of large bulk densities, i.e. we study the system's performance for large values of α and $\beta \ll 1$. For this case one expects to find frequently a compact cluster of particles at the right boundary. Therefore the mean time interval for a particle leaving the system is the sum of the average waiting time $T_L = 1/\beta$ of the last particle at site L and the average time which passes until the last site is occupied again, $T_J = 1/q_0$. One finds immediately that for large $\alpha \approx 1$ and $\beta \ll 1$ the flow is given by

$$J(\beta) = \frac{1}{T_L + T_J} = \frac{q_0\beta}{q_0 + \beta}. \tag{6.5}$$

This simple scenario is only valid if the density of holes fed into the system is very low. For larger values of β one expects that it is also possible that the cluster separates from the right boundary. In this case the density close to the exit is determined by the outflow from a cluster. The temporal headway t between two consecutive particles is distributed via $P_h(t) = q_0(1-q_0)^{t-1}$ where $t \geq 1$. Now we calculate the typical amount of time which is needed from the arrival of a particle (at $t = 0$) to the arrival of the second particle at ($t = T$) at site L. Here we have to distinguish two cases: (i) the particle arrives at site $L-1$ *before* the first particle has left the system or (ii) that it arrives later, such that it reaches the last site without being blocked by the particle ahead. The probability that a particle gets blocked if it arrives at t is given by $P_b(t) = (1-\beta)^t$ and that it can pass without blockage by $P_f(t) = \sum_{\tau=1}^{t} \beta(1-\beta)^{t-1}$.

This leads to the average value of T given by

$$\begin{aligned} T &= \sum_{t=1}^{\infty} P_h(t)\left[P_f(t)(t+1) + P_b(t)(t + \frac{1}{\beta} + \frac{1}{q_0})\right] \\ &= \frac{1}{\beta} + \frac{1}{q_0} = J(\beta)^{-1}. \end{aligned} \tag{6.6}$$

Also for this scenario we recover the same value (6.5) of the flow. These two kind of configurations are generic if the output probability controls the capacity of the system, i.e. in the presence of clusters. Therefore we expect to find a unique functional dependence of the flow, if the system is controlled by the capacity of the exit. The transition between the α or β controlled parameter regime is expected to be located at

$$\beta_t(\alpha) = \frac{q_0\alpha}{(1+\alpha)q_0 - \alpha} \tag{6.7}$$

where both fluxes agree.

Comparison of the prediction for the flow with simulation results shows excellent agreement. Simulations for different lengths of the chain show that the differences between these predictions and the simulations systematically vanish for larger system sizes. The origin of these finite size effects, i.e. the enhancement of the flow for large β, is the possibility to find occasionally cluster-free micro-states. This is indicated by the broken lines in the phase diagram (Fig. 6.5). The absence of maximal current phase in the thermodynamic limit is related to the non-analyticity of the fundamental diagram [7].

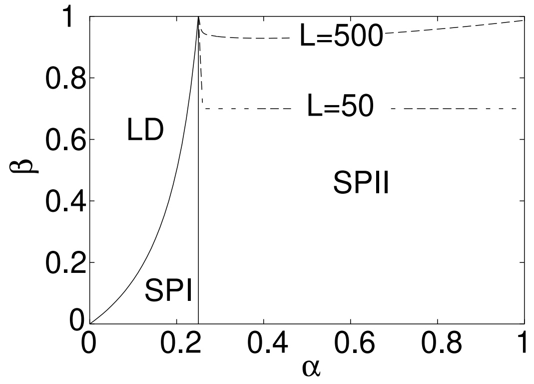

Figure 6.5: Phase diagram of the open system for $q_0 = 0.25$. The phases are in order: low density phase (LD), striped phase I (SPI), and striped phase II (SPII). At the line $\alpha = q_0$ one observes a constant density profile. The dashed lines show parameter regimes where in finite systems a systematically larger flux has been observed. (From [22])

The typical microscopic structure of the stationary state can be characterized by in- and outflow rates α and β. One can distinguish three different domains, i.e. a *low density* domain (LD) for $\beta > \beta_t(\alpha)$ (LD), and two high density domains for $\beta < \beta_t(\alpha)$. Both high density domains correspond to a *striped phase* (SP), but they exhibit different behaviors in the vicinity of the entrance, depending whether $\alpha < q_0$ (SPI) or $\alpha \geq q_0$ (SPII). In the LD phase one can observe the typical two domain structure known from the asymmetric exclusion process. Clusters which eventually separate from the high density domain at the right dissolve in a few time steps. This dissolution leads to the localization of the high density domain at the right. The system takes a bulk density $\rho_b(\alpha) = J(\alpha)$. At site L the density is given $\rho_L = J(\alpha)/\beta$. Fits of several density profiles follow the pure exponential form $\rho(n) = \rho_b(\alpha)+[\rho_L-\rho_b(\alpha)]\exp(-(L-n)/\xi)$.

In the high density region (SPI + SPII), clusters are able to reach entrance. This region can be described by considering that at the right boundary, some free-flow segments are injected within a compact cluster. Typically, the free-flow segments reduce to isolated holes for $\beta < q_0$, whereas for $\beta > q_0$, they contain both empty sites and particles with velocity one.

Chapter 7

SK-model with open boundary conditions

7.1 Introduction

After presenting some known Models and results, we would like to study the SK-model (described in chapter 5) with open boundary conditions. The goal is to find a crash free system with open boundaries and to study different phases of the system as well as *current-density* relations.

As we saw in chapter 5, the SK-model defines a safe velocity v_{safe} for each car, which is a function of velocities of this car and the preceding car, the gap g between these cars and the maximum deceleration b of the Model. The v_{safe} is defined as:

$$v_{safe} = v_l(t) + \frac{g - v_l(t)}{\frac{v_f(t)+v_l(t)}{2b} + 1} \tag{7.1}$$

This is the maximum safe velocity for the following car and guarantees that there are no crashes between the following and the preceding cars.

For the injected car however, one has to find another way to define a safe velocity, which has to be a function of known parameters in the system, i.e. velocities and gaps of the existing cars in the system. In other words, one should find an initial velocity v_{init} for a car, being injected , which guarantees the crash-less travel of this car in any time step. The injected car would travel free of crashes, if the driver can, under any circumstances, bring the car to a complete stop before colliding with the preceding car. That means, if the driver has a reaction time τ and the braking distance of the cars from velocity v is given by the function $brake(v)$, the situation is safe, if

$$brake(v_{\mathrm{f}}) + v_{\mathrm{f}}\tau \leq brake(v_{\mathrm{l}}) + g \; . \tag{7.2}$$

The safety in the SK-model is guaranteed for any t if $g(t = 0) \geq v_l(t = 0)$. This means, that the *gap* between the injected car and the first car in the system should be at least as big as the velocity of the first car in the system.

Using this safety condition introduced by the SK-model, it is impossible to inject cars in the system with a rate, only depending on α. Another problem dealing with this safety condition is the maximum *current*. Using this condition, the system would not reach a maximum *current* comparable with systems with periodical boundary conditions. (See chapter 9.)

This is the reason why we have studied systems with several injecting rules. In chapters 8 and 9 the results of the studies we have made to understand the dynamic of a system, using the SK-model with open boundary conditions and different injecting rules, are explained. In chapter 8 we have tried to inject cars with the injecting rate α, with a safe velocity $v_{init} > 0$. In chapter 9 we have tried to inject cars with the velocity v_{max} in the system, which means that, we could not inject cars with the injecting rate α.

In the following sections we have used the following parameters for the simulations.

$$\begin{aligned} a &= 0.1 \\ b &= 0.6 \\ v_{max} &= 5 \\ \epsilon &= 1.0 \\ l_{car} &= 1.0; \end{aligned} \tag{7.3}$$

Chapter 8

An injection rule oriented on the inflow rate α

8.1 Introduction

In this section we introduce an injection method, which is oriented on the inflow rate α. It means we try to inject cars , with the injecting rate α, in the system with any safe initial velocity (depending on the system configurations). We would like to inject the cars with a maximum safe velocity to reach a maximum *current*. We will show, this is not easy and one has to deal with some problems. First an overview of the open boundary conditions and update rules is given.

Open boundary conditions in these simulations are defined in the following way:

Step 1: Injection
With probability α: if there is at least one car length free space at the beginning of the system, we inject a car with velocity v_{init}. v_{init} is a function of v_{max}, the velocity of the leading car(v_l), b which is introduced in the SK-model in chapter 5 and the maximum reachable deceleration for the leading car (b_l), which is calculated, using the velocities of preceding cars.

If $v_{init} \geq v_{max}$, we use v_{max} for the velocity of the injected car.

Step 2: First update and definition of the v_{crit}
For the injected car, for the first update, we look if the leading car has a velocity bigger than v_{crit}. If so we follow the normal SK-model update rules, if not we set the velocity of the injected car to the *gap* to the preceding car. This help us to avoid crashes in the system, which is a big problem for this injecting method and will be explained in section 8.2.

Step 3: Extraction
With probability $1 - \beta$: we add a block at the end of the road which causes a slowing down of the cars

at the end of the system. Otherwise, with probability β, the cars simply move out of the system.

Step 4: Update
Update with the SK-model update rules (See chapter 5).

In this section, v_{crit} is chosen to be 1.6 , v_{max} is 5 , $a = 0.1$ and $b = 0.6$.

8.2 Safe velocity for injecting cars

In this subsection, a method to find a plausible safe velocity for an injected car is described.

Newton braking distance for a constant deceleration is defined as :

$$brake(v) = \frac{v^2}{2b}. \tag{8.1}$$

One can easily extract this equation using equation:

$$\frac{dv}{dt} = b. \tag{8.2}$$

and the equation of motion:

$$dx = vdt. \tag{8.3}$$

Integrating this equation one gains:

$$\Delta x = \int_0^v v_1 dt = \int_0^v \frac{v_1 dv_1}{b} = \frac{v^2}{2b}. \tag{8.4}$$

Using the Newton's braking distance -under the circumstance that both cars have the same deceleration b and τ is one time unit of the system - the safety condition (equation (7.2)) for the injected car , which should have the initial $v = v_{init}$, will be:

$$\frac{v_{init}^2}{2b} + v_{init} = \frac{v_l^2}{2b} + g. \tag{8.5}$$

Solving this equation for v_{init} one will have:

$$v_{init} = \sqrt{2bg + v_l^2 + b^2} - b. \tag{8.6}$$

The assumption that both cars have the same deceleration b is not acceptable. Note that the b_{max} introduced in the SK-model could be violated and there is no constraint forcing the cars having a deceleration rate smaller or equal to b_{max}. This means, it could happen that the leading car has a bigger $b = b_l$ than deceleration b of the following car. One can extend the equation (8.6), calculating the maximum $b = b_l$ for the leader, possible from the situations in the system at time step t. The maximum reachable $b = b_l$ for the leader is: $b_l = v_l(t) - v_l(t+1)$ with the assumption that $v_l(t+1)$ is a minimum reachable velocity for the leader, which is $min(v_{max} - a, v_{safe} - a)$. Solving the safety condition (equation (7.2)) one gains again:

$$v_{init} = \sqrt{2bg + \frac{b}{b_l} v_l^2 + b^2} - b. \tag{8.7}$$

With $b_l = max(b_{max}, v_l - min(v_{max} - a, v_{safe} - a))$, which is a function of v_l and v_{safe} for the leading car.

Note that for the SK-model the time is discrete and in each time step the values like v_{safe} are calculated from the system parameters. It means a car could have quite different values of b for an interval δt causing the braking distance become a non-deterministic value. As we saw the b is also not limited with the SK-models maximum deceleration b_{max} and could vary from 0 to a actual real maximum value of $b_{maximum} = v_{max}$, this could happen when a car slows down and stop in just one time step. This means our approximation for the v_{init} does not guarantee a safe situation.

There are several methods solving this problem. After trying different methods, making the v_{init} safe, because of our interest, gaining the highest available current in the system, we decided to use the following method:

We check if the leading car has a minimum velocity of v_{crit} or not. If so we follow the normal SK-model update rules, if not we set the velocity of the injected car to the gap to the leading car.

It is plausible to search for the smallest v_{crit}, for which the system remains free of crashes. For a system with $v_{max} = 5$, it was observed (from several simulations), that for a $v_{crit} \geq 1.6$ no crashes happens anymore.

8.3 Stationary state

For simulations, it is important to have a knowledge of the number of time steps, for which the system reaches a stationary state. In this section we study the system to find out about the number of the time steps one has to deal with, to run the simulations, before reaching the stationary state. We will refer to this number of time steps as *relaxing time*.

The relaxing time could be a complicated function of α , β and *Length* of the system.

There are several methods estimating a relaxing time. The estimations are not the same and depend on the method one has used. Three methods are described here:

i) One could study the time evolution of jams in a $x{-}t$ diagram. To reach the stationary state, one should wait for the jams to reach the beginning of the system.

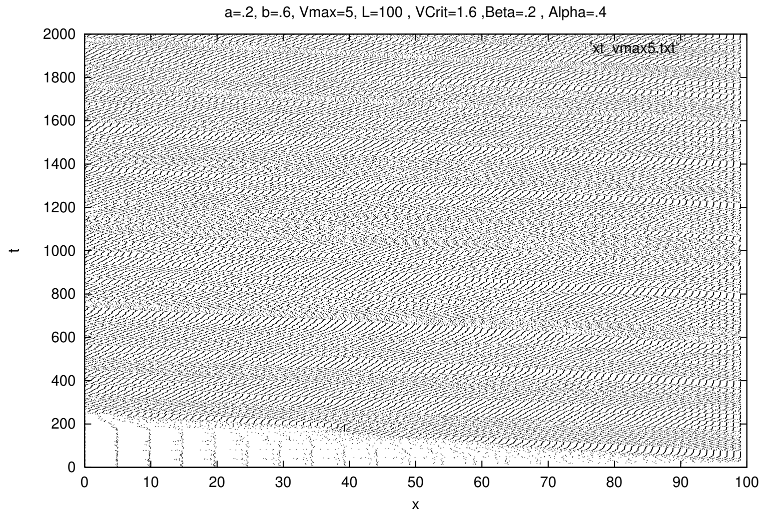

Figure 8.1: Time evolution of jams. The jams need about 250 time steps to reach the left border. In this example β is 0.2 and the length of the system is 100. The velocity of upstream growing jams is about $11\frac{km}{h}$, which is comparable with the empirical data.

Fig. 8.1 shows the time evolution of jams in a $x - t$ diagram for a very small system ($Length = 100$). The jams need about 250 time steps to reach the left border. In this example β is 0.2, it means just 20 percent of cars are allowed to leave the system. This causes jamming situations in the end of the system, which moves upstream with velocity of about $\frac{0.4 * l_{cal}}{1 sec.} = 3\frac{m}{s} = 11\frac{km}{h}$, which is comparable with the empirical data.

ii) One could measure the current somewhere in the system and see if it changes in time. Fig. 8.2. shows the time evolution of the *current* measured in the middle of the system for different relaxing times and different pairs of (α, β). In this example the *current* reaches a constant value, first after a minimum of 12000 time steps.

The current reaches actually a stationary state as some other parameters in the system are changing in time, causing the system to be not in a real stationary state. For example as the plateau in a density profile changes in time, the *current* remains constant. This means, in order to measure ρ using density profiles one should deal with other relaxing times. This will be explained in *iii*).

iii) To examine if the system is in stationary state one could measure a density profile for a pair of (α, β) using different relaxing times. In Fig. 8.3 we show how the densities of different positions in the system change in time an get close to a constant of 0.64. For a better comparison one can see the Fig. 8.4.

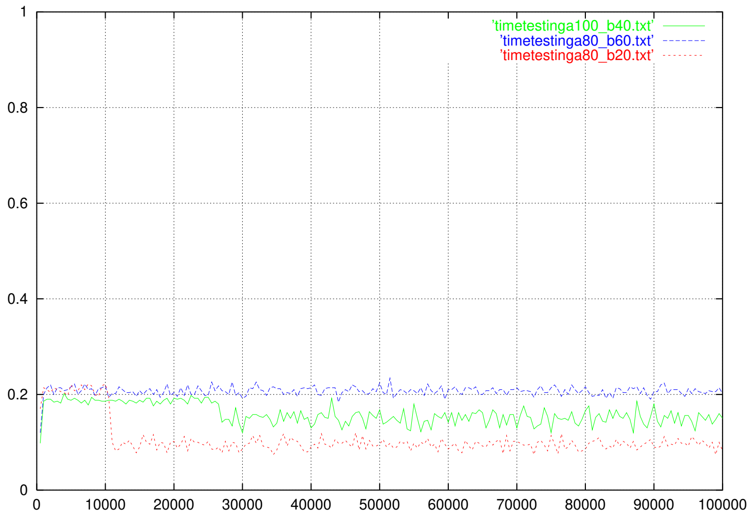

Figure 8.2: Time evolution of the current. The *current*, measured in the middle of the system, reaches a constant value, first after a minimum of 12000 time steps. The lines are the measurements for different (α, β) pairs.

8.4 Relations between α, β and the current, the average velocity and the density

The dynamics of a system with open boundary conditions depends on α and β parameters. With increasing α , one tries to inject more cars, which causes a higher *current* first. With $\alpha \geq 0.58$ a jamming situation will be formed at the beginning of the system which causes a lower average velocity, lower input and respectively lower *current* in the system. In chapter 9 we will introduce another injecting strategy, which help avoiding decrease of *current* with increasing α .

In Fig. 8.5 an $\alpha - current$ diagram for a system with $\beta = 1.0$ is shown. The *current* (q) increases with α monotonously first and reaches the maximum of about 0.6. For $\alpha \geq 0.58$ one has to deal with jams at the beginning of the system, which causes the *current* to decrease and reach the value of 0.2.

With decreasing β, the cars at the end of the system are forced to slow down and stay in the system, this causes a jamming situation at the end of the system, which grows backwards. In this case the cars have a lower average velocity, the density of the cars in the system is higher. This means, for different pairs of (α, β) one can expect different nontrivial dynamics. This will be discussed in section 8.6.

The relation between α and the *current* for several β's is shown in Fig.8.6. It is obvious that the *current* decreases for smaller β's.

Because of the metastability, the system has a quite different behavior for $\beta = 1.0$ in comparison to any other β. Any small perturbation in the system forces the system goes out of the metastable situation. A jamming situation ($\beta \neq 1.0$) causes a decrease of the *current*. Note that the system has even a quite

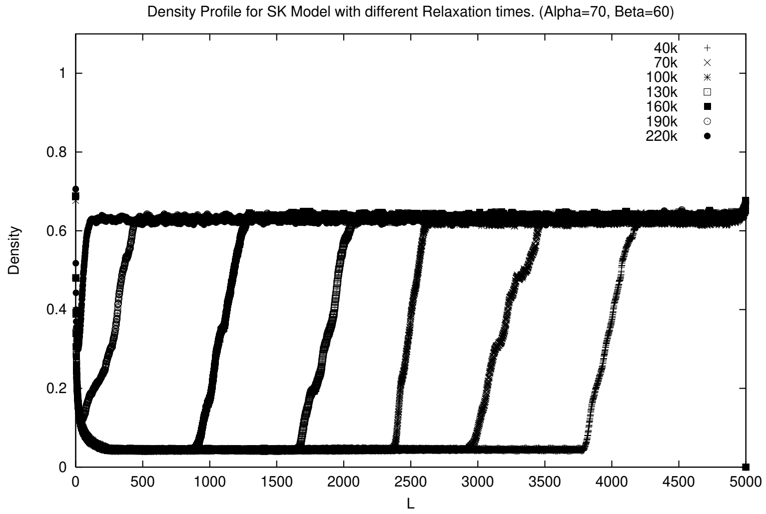

Figure 8.3: Time evolution of the density profiles. The plateau grows and reaches a value of 0.64. The points are measurements of the densities of positions. Different relaxing times are used. The plateau grows with an almost constant velocity. For more details see Fig. 8.4

different $\alpha - current$ relationship for $\beta = 0.95$.

In Fig. 8.7 a separate $\alpha - current$ diagram for a systems with $\beta = 0.7$ is shown.

On the other hand, one can study the relationship between *current* and β, using a constant value of α. It is obvious that for very small values of β, the *current* should vanish. In a system with closed right boundary, almost all cars are forced to stay in the system. This means a very low average velocity (almost $\langle v \rangle = 0$) and very high density (ρ is close to 1). For each α value, one expects the highest value of *current* for $\beta = 1$. These are shown in Fig. 8.8.

The *current* is a function of the average velocity and the global density. It is interesting to have a knowledge of the relationship between these values and (α, β) parameters.

For $\beta = 0.8$, the relation between average velocity $\langle v \rangle$ and α is shown in Fig. 8.9. For $\alpha < 0.25$ and $\alpha \geq 0.6$ the average velocity $\langle v \rangle$ is very close to 4.95 (See section 8.6). For other values of α, the $\langle v \rangle$ is much smaller and is about 0.5.

In Fig. 8.10 the relation between density, measured in the middle of the system [1]and α for the same parameters is shown. For $\alpha \geq 0.25$ and $\alpha < 0.6$ the density ρ is about 0.5. For other values of α, the density is much smaller and is about 0.05.

In Fig. 8.11 the average velocity as a function of α and β is shown. The contours show the lines of constant $\langle v \rangle$. One can distinguish between two different phases, namely the free flow phase with $\langle v \rangle$

[1]In all following simulations, the density is a mean value of densities of a finite interval of $\frac{L_{system}}{3}$ located in the middle of the system.

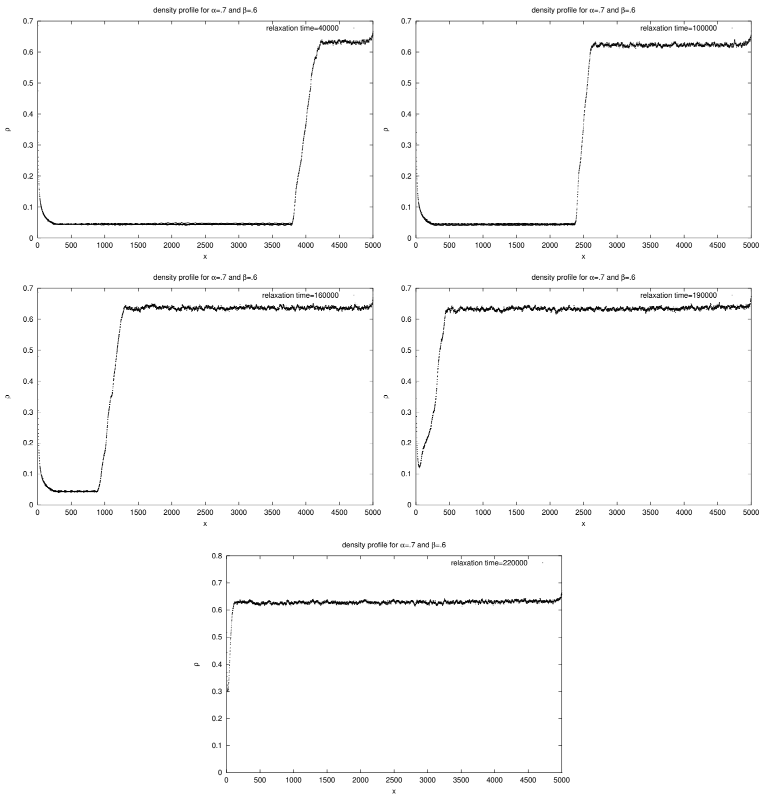

Figure 8.4: Time evolution of the density profiles (see Fig. 8.3). Relaxing Time =40000-220000 in 60000 steps

close to v_{max} and jamming phase with $\langle v \rangle$ much smaller than v_{max}. In section 8.7 we will explain another method of finding the phase diagram, using the density profiles.

In Fig. 8.12 the density, measured in the middle of the system, ρ as a function of α and β from two other view angles are shown. The contours show the lines of constant ρ. One can distinguish between two different phases, namely the low density phase with $\rho < 0.15$ and high density phase with ρ close to 1.

It is interesting to compare the contours from these figures and those from the Fig. 8.11. They both look similar and similar to the phase diagram drawn using the density profiles (see section 8.7).

8.5 The fundamental diagram

The fundamental diagram (FD) shows the relation between global density and *current*. In comparison to periodical boundary conditions, it is difficult to find a fundamental diagram for the systems with open boundary conditions. In systems with periodical boundary conditions it is possible to choose a ρ, run the simulation and measure the *current*. For systems with open boundary conditions, one has to start a

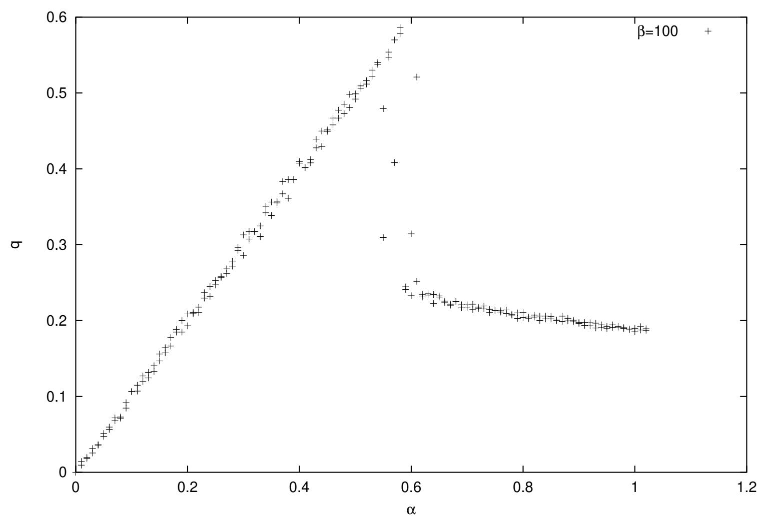

Figure 8.5: $\alpha - current$ diagram for a system with $\beta = 1.0$ is shown. The *current* (q) increases with α monotonously first and reaches the maximum of about 0.6. For $\alpha \geq 0.58$ a jamming situation is formed at the beginning of the system, which causes the *current* to decrease and reach the value of 0.2.

simulation with the tuning parameters α and β, which do not have a linear influence on ρ or *current*.

Global density and *current* should be measured in stationary state. As we saw, for certain pairs of (α, β), a system reaches the stationary state after a long simulation time. So one has to deal with two difficulties finding a FD, first the simulation time should be very large and second, there is no guarantee that the FD has no hole (See Fig. 8.13.). Because of the complex relation between of (α, β) pairs and ρ or *current*, one can not find a value for the *current* for each ρ and vice versa. As we saw in the last subsection, ρ and *current* are extreme sensible against changes in α or β.

Our strategy finding the FD is:

To find the relation between ρ and *current* one should choose a pair of tuning parameters α and β, let the system run for a certain time depending on α and β to reach the stationary state. When there is enough evidence that the system is in the stationary state (see section 8.3), one can measure ρ in the middle of the system and *current* through the system. These two values would fix a point in the fundamental diagram. To make the data more secure and avoid noises, one should repeat this process for several systems and gather more points for each (α, β) pair.

One of the diagrams generated with this method is shown in Fig. 8.13. There is a hole in the density interval $0.16 < \rho < 0.38$ in this diagram. Note that the density and the *current* are measured in the middle of the system. In next section we will show another diagram using the information of the density profiles.

The form of the fundamental diagram can be easily understood. For small densities all cars move with a velocity close to v_{max} causing the *current* increase monotone. For bigger densities the cars interact

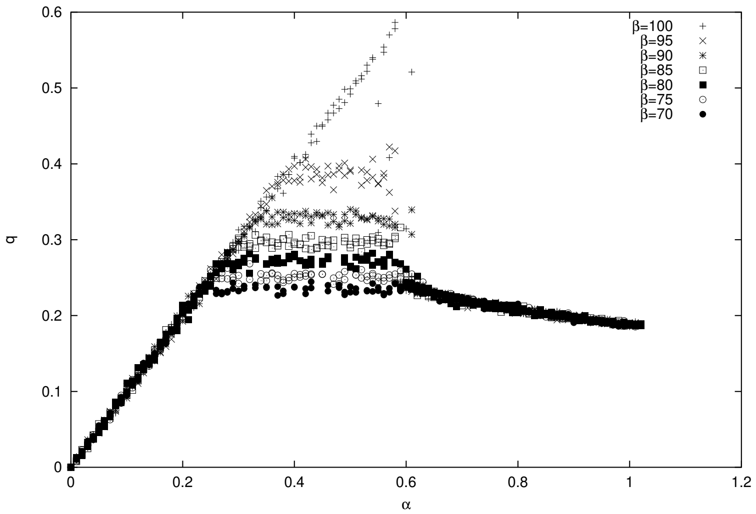

Figure 8.6: $\alpha - current$ diagram for $\beta \in [0.70, 1.00]$. the *current* decreases for smaller βs due to the jamming situation at the end of the system.

with each other and the mean velocity is much smaller than the free flow regime. this causes a decrease of the *current*.

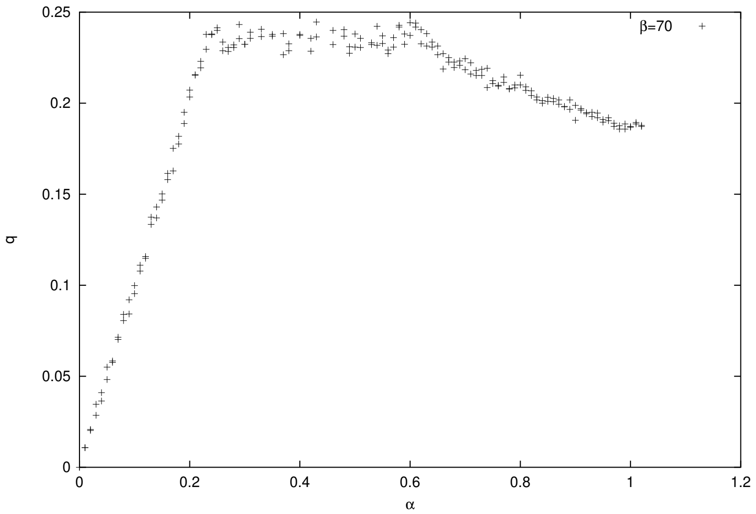

Figure 8.7: α - *current* diagram for β = 0.7.

8.6 Density profiles

A density profile , calculated for a system in the stationary state, has information about the phase of the system and the distribution of densities in the system. Possible phases are low density, high density and maximum current phase (see section 6.2). As we saw in section 6.2, phases of a system are usually described in terms of α and β. One could try to describe the phases of a system in terms of densities at the beginning and at the end of the system.

Having density profiles, one can draw a phase diagram, which explains the phases and phase transition behaviors of a system. This will be down in section 8.7.

In this section, we explain the different types of density profiles, structure of a density profile and the dependence of a density profile on α and β. In this section, all the simulations are made with systems with Length of $2001 l_{car}$ units. The relaxing time is chosen to be 2000000 time units and the quantities are the mean values of 20000 time units measurements.

In Figs. 8.14 and 8.15 two typical density profiles for low- and high density phases are shown. The characteristic difference is the density of the plateau. In the low density phase, the plateau of the density profile has a density smaller then 0.1. In the high density phase however, the plateau of the density profile has a density bigger than 0.15. In the maximum current phase, we measured densities between 0.1 and 0.15.

For a system with open right boundary (β = 1) and low injection rates (α < 0.65) the density profiles are characterized by a periodical structure (see Fig. 8.16). One can distinguish between two structures, namely the oscillations with peaks each 5 positions (see fig. 8.17), and a larger oscillation with peaks each 99 positions.

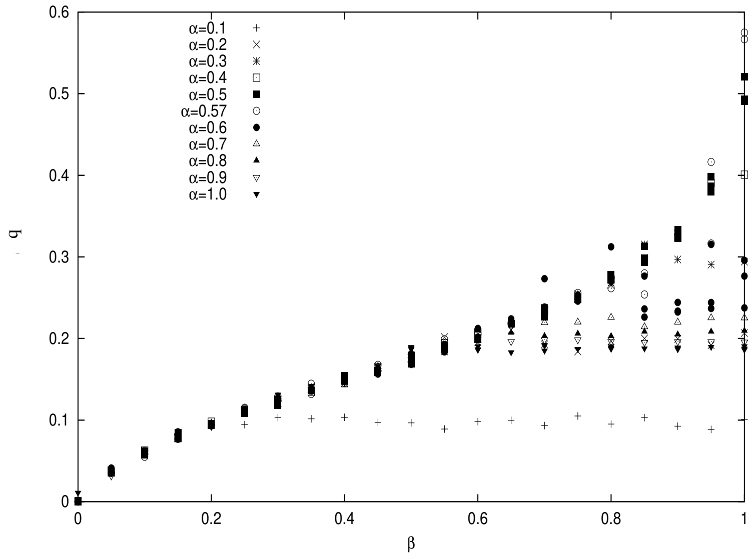

Figure 8.8: β - *current* diagram for $\alpha \in$ [0.1, 1.00]. The *current* vanishes for very small values of β.

The oscillations depend on the model-parameters of a system, like a and v_{max} and the size of bins one uses to measure the densities. To understand this structures we consider a density profile for a system with open right boundary ($\beta = 1$) and a very low injection rate of $\alpha = 0.1$.

For $\alpha = 0.1$ the probability of generating a car at the beginning of the system ($x = 0$) in two successive time steps is very small ($p = 0.01$). It means with a very larg probability ($p = 0.99$), the cars have no interaction at the beginning of the system. These injected cars are created at the beginning of the system with the initial velocity $v_{init} = v_{max} = 5$ (see section 8.1). As we saw, the SK-model has a randomization step, each car will be slowed done by a random amount η that is uniformly distributed between 0 and ϵa, where ϵ is a parameter between 0 and 1. In our simulations ϵ is chosen to be 1.

Using the update rules (equation (5.19)), one can calculate the mean value of the velocity of N cars for a time t as:

$$\langle v \rangle_t = \frac{\sum_{n=0}^{N} v_n}{N}; \tag{8.8}$$

As we saw for very low injecting rates, the safe velocity in any time is v_{max} . So one can rewrite the equation (8.8) as:

$$\langle v \rangle_t = \frac{\sum_{n=0}^{N} v_{max} - \epsilon \eta_n}{N} = v_{max} - \sum_{n=0}^{N} \epsilon \eta_n = v_{max} - \epsilon \int \eta_n dn = v_{max} - \frac{\epsilon a}{2}; \tag{8.9}$$

In our model with parameters $v_{max} = 5$, $\epsilon = 1$ and $a = 0.1$ the average velocity $\langle v \rangle$ is 4.95.

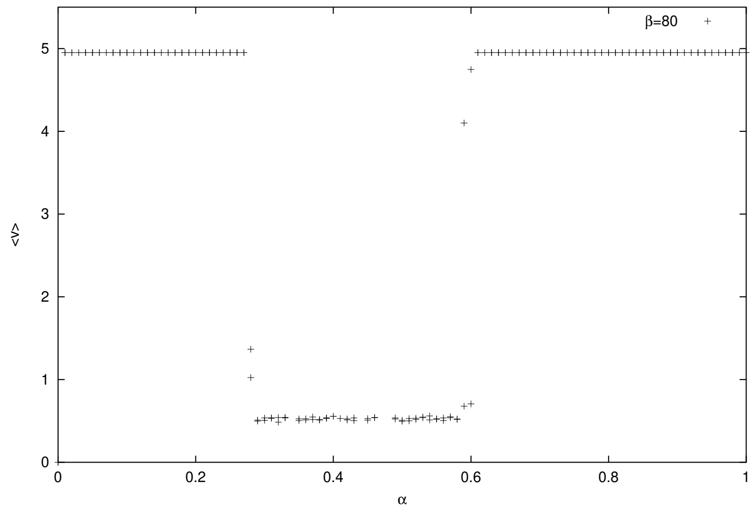

Figure 8.9: α - average-velocity diagram for a system with $\beta = 0.8$. For $\alpha\langle 0.25$ and $\alpha \geq 0.6$ the average velocity $\langle v \rangle$ is very close to 4.95. For other values of α, the $\langle v \rangle$ is much smaller and is about 0.5.

The injected cars move to the position $x = 4.9$ or $x = 5$ at the next time step depending on the random number η in this time step. From the statistical point of view, for a very large number of cars and measurements the probability to find these cars on $x = 4.95$ at the next time step is much bigger than the probability of finding them on any other positions between 4.9 and 5.

To measure the density profiles, we look the position of each car x_n, increase the occupation value (initial value = 0) of the biggest integer number, smaller or equal to x_n (in this method the bin length is also one l_{car}). For example if a car has a position $x = 64.7$ we increase the occupation value of bin $i = 64$. We repeat this measurement for a long period of time T and then calculate the mean value of occupations as ρ.

As a general formulation, one can write:

$$\rho_x(Bin) = \frac{\sum_{n=0}^{N}\sum_{t=0}^{T}\delta(integer_{Bin}(x_n)-x)}{T.Bin}. \tag{8.10}$$

with x=0, x+Bin , x+2Bin ,..., x+nBin.

Where Bin is the size of the bins one uses to measure the occupation. The $integer_{Bin}(x_n)$ denotes the smallest multiplication of Bin, smaller than x_n. For example $integer_5(23.2)$ is 20.

For measurements with $Bin = 1$ one expects that the first bin ($i = 0$, $x \in [0, 1)$) should contain no car in any time step and the ρ should be 0[2]. The bins $i = 1, 2, 3$ should also be empty because of the non-

[2]Creating and moving are parallel and in one time step.

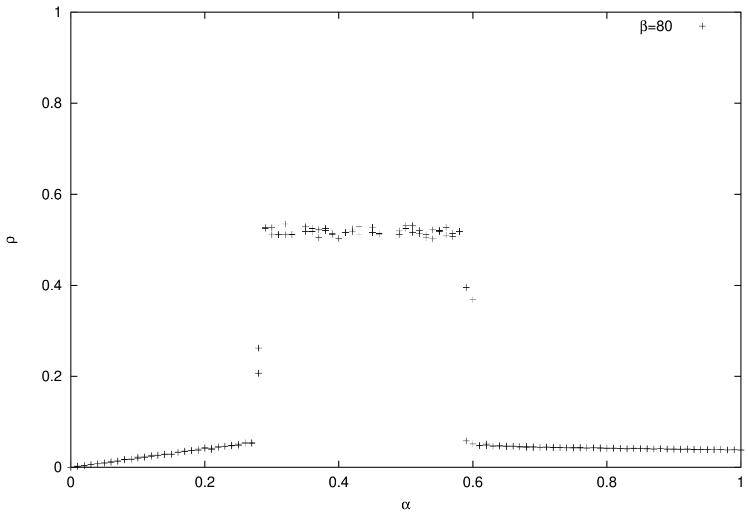

Figure 8.10: $\alpha - \rho$ diagram for a system with $\beta = 0.8$. For $\alpha \geq 0.25$ and $\alpha < 0.6$ the density, measured in the middle of the system ρ is about 0.5. For other values of α, the density is much smaller and is about 0.05.

interacting nature of the low-injecting-rate systems, in which the cars are traveling with a velocity close to v_{max} . Also the next bin with a non-vanishing ρ should be the bin with $i = 4$ ($x \in [4, 5)$). Using this argumentation one expects to have every 5 bins, a bin with a non-vanishing ρ. Also for bins $i = 4 + 5n$ we expect non vanishing densities. If we use bins length of 5 instead 1 we expect naturally the same result. The only difference is the occurrence of the measurements, with other words one can decide how much he would like to zoom and see the details.

In Fig. 8.17 we have shown the density profile for a system with $\beta = 1$ and $\alpha = 0.1$ and bins length of 1.

In our example, an injected car traveling with $velocity = \langle v \rangle$ will be on position $x = 99$ after 20 time steps and after 21 time steps it will be on position $x = 103.95$ which means that the bin with $i = 103$ will have a non-vanishing density ρ. Also we have to deal with a period of 99 l_{cal} for the oscillation. It is obvious, that our choice of $a = 0.1$ causes the period of 99 car lengths. With $a = 2$ one should expect a period of 49 car lengths. In this case $\langle v \rangle$ will be 4.90, and after 10 time steps the position would be $x = 49$, however the position for the last time step was $x = 44.1$ causes the bin $i = 44$ to have a non-vanishing density. This is repeated each 10 time steps (49 position units).

In figures 8.18 and 8.19 these periods are shown.

As we saw In Fig. 8.17, the probabilities to find a car in bins with $i = 5n, i = 1 + 5n, 2 + 5n, 3 + 5n$ for small ns are vanishing (forbidden positions). This would not be the same for bigger values of n . After enough time steps, the summation of probabilities of braking due to the randomization step will be large enough to cause a car be on a position other than $i = 4 + 5n$. For an absolute non-interacting system, the first bin, out of the group of main bins ($i = 4 + 5n$), with a non-vanishing occupation probability would

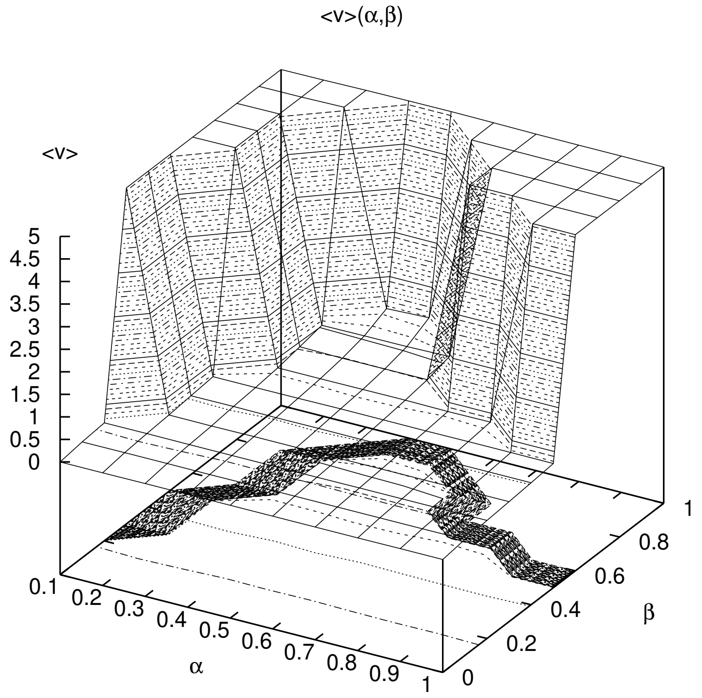

Figure 8.11: Average velocity as a function of α and β. The contours show the lines of constant $\langle v \rangle$. One can distinguish between two different phases, namely the free flow phase with $\langle v \rangle$ close to v_{max} and jamming phase with $\langle v \rangle$ much smaller than v_{max}.

be the bin with $i = 28$. Suppose an injected car has to brake each time step due to the randomization (the probability is very small indeed but not zero), so this car would be on position $x = 4.9$ in the first time step, on $x = 9.7$ in the second time step and on $x = 28.9$ in the sixth time step which means the bin with $i = 28$ would have a non vanishing value in the density profile.

For low-interacting systems (bigger α's but $\beta = 1$) the probability to find cars on any position (except forbidden positions) would increase (See Fig. 8.20). In this figure, each position with $x \geq 15$ has $\rho > 0$.

For high-interacting ($\beta \ll 1$) systems one expects no oscillations anymore. In such systems the probability of finding cars on any position is a constant (depending on β). Because of high interactions, the cars have to match their velocity to each other and the average velocity would be much smaller than v_{max}, which causes ρ be a continuous function of x or i. (See Fig. 8.21).

One can use other bin lengths to avoid measuring the oscillations, to have a knowledge of mean occupancy. In Fig. 8.22 one can see the same density profile with two different bin lengths (*Bin*) of 1 and 5.

8.7 Phase transitions and phase diagram

In the ASEP, it is usual to use $\alpha - \beta$ plane for a phase diagram. To find the phase of a system as a function of α and β one should study the density profiles. It is easy to distinguish between low- and high-density phases. To find the maximum current phase, one should compare the (ρ, *current*) pair of the system with the FD of the same system with periodical boundary conditions.

In Fig. 8.23 the FD of a system with periodical boundary conditions and the same system with open boundary conditions is shown. Black points are coming from density profiles of the system with open boundary conditions. The metastable branch does not exist for the system with open boundary conditions. There is also a hole in the FD of the system with open boundary conditions.

To have more points, one should measure density profiles for more (α, β) pairs. Note that these simulations are long time running programs.

Using the density profiles for systems with α's and β's between (0, 1) each 0.1 increments, we have drawn a phase diagram in Fig 8.24. Different phases, phase transition regions and the typical density profiles for each phase are shown. The maximum current phase with *current* about 0.5 has been observed for system with open right boundary ($\beta = 1$) and injection rate between $\alpha = 0.48$ and $\alpha = 0.57$.

This phase diagram looks different from other phase diagrams for similar models. That's a motivation why we used other injecting strategies.

We have also tried to examine the extremal-principle (see sec. 6.2) to describe the phase diagram. For small injection rates, it is not easy to find the left boundary density ρ^-, due to the oscillations. For a system with $\alpha = 0.70$ and $\beta = 0.6$ we measured the boundary densities $\rho^- = 0.3$ and $\rho^+ = 0.65$ (see. Fig. 8.4). From the fundamental diagram of the periodic system (Fig. 5.2), we will have $j^+ = 0.2$ and $j^- = 0.38$. According to (6.2) the shock travels with speed $v_s = (j^+ - j^-)/(\rho^+ - \rho^-) > 0$ to the right, making the bulk density equal to ρ^-. this could be seen in Fig. 8.4. According to (6.4) the current will be equal to $min(j^+, j^-) = 0.2$. This is in agreement with the current we have measured in long time simulations.

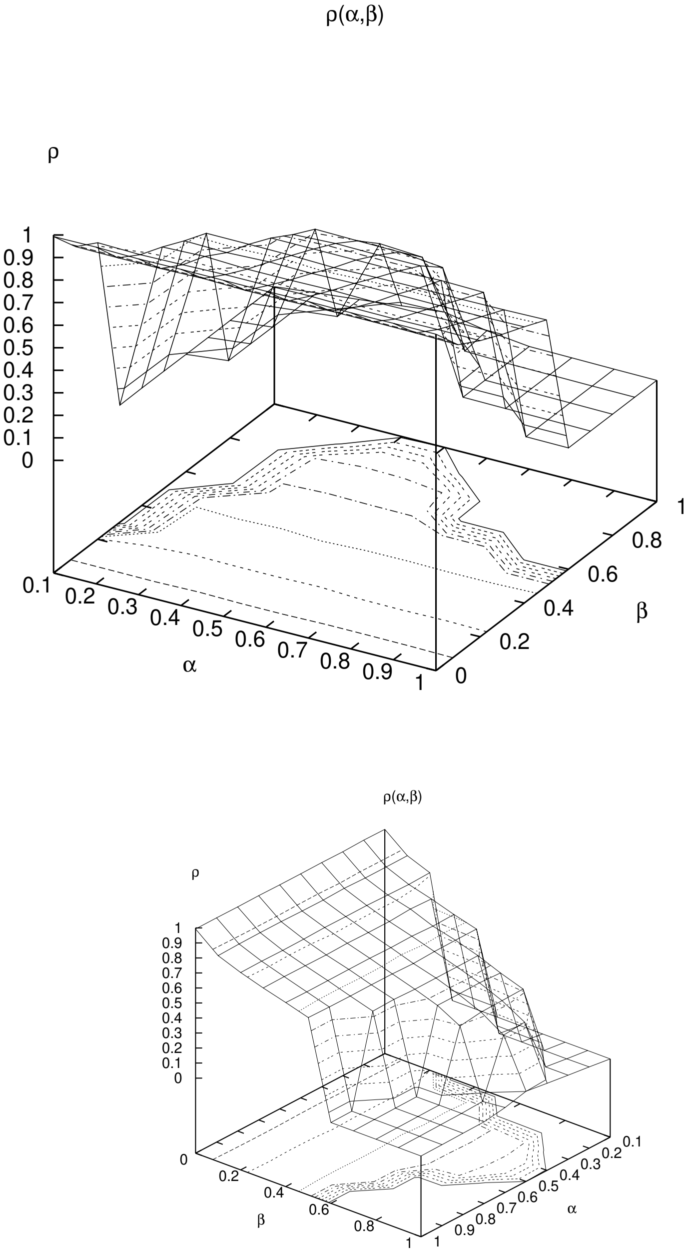

Figure 8.12: Density, measuered in the middle of the system, as a function of α and β. The contours show the lines of constant ρ. One can distinguish between two different phases, namely the low density phase with $\rho < 0.15$ and high density phase with ρ close to 1.

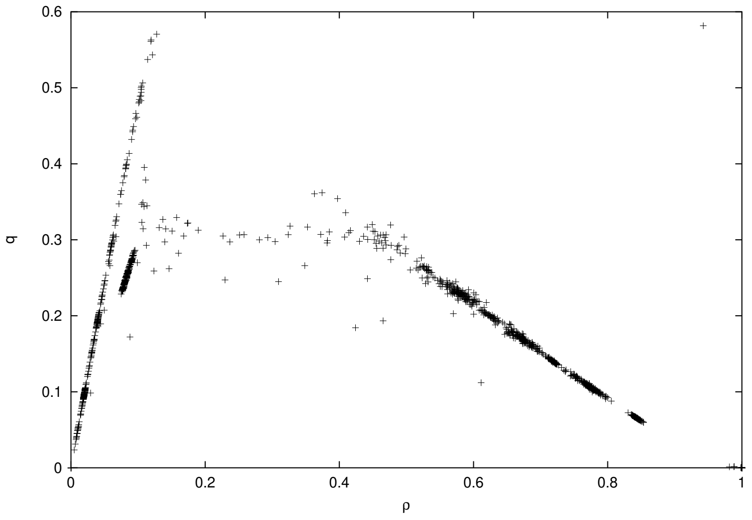

Figure 8.13: Fundamental diagram, using long time simulations. The density and the *current* are measured in the middle of the system. There is a hole for the density interval $0.16 < \rho < 0.38$ in this diagram due to the drastic decrease of the *current* with increasing of α.

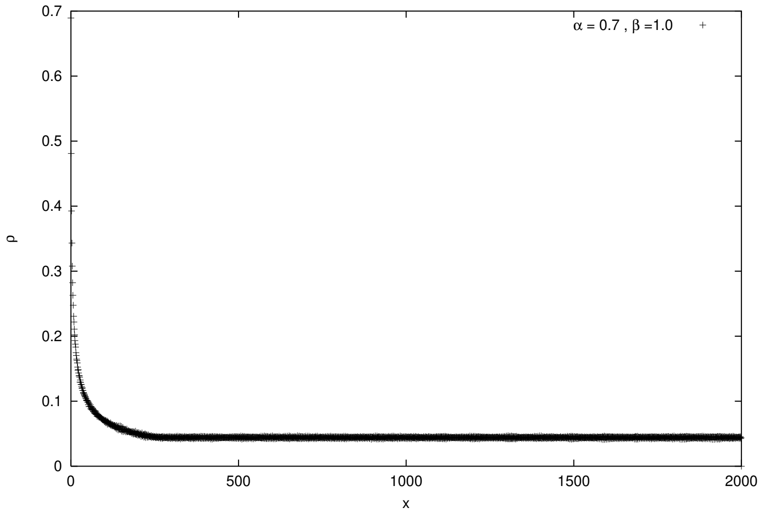

Figure 8.14: Density profile for a system in the low density phase.

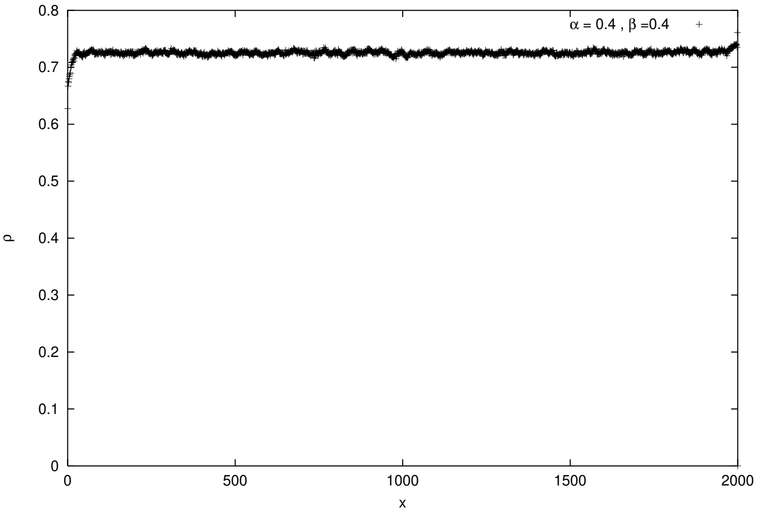

Figure 8.15: Density profile for a system in the high density phase.

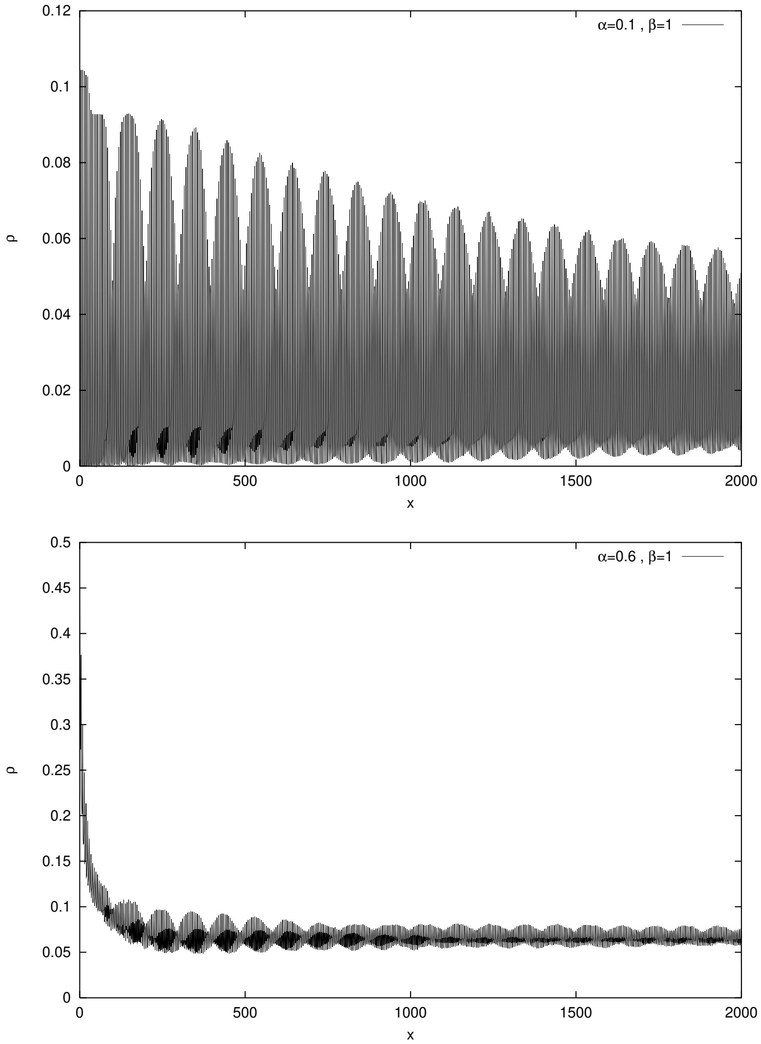

Figure 8.16: Density profiles for a system with open right boundary and low injecting rates. The density profiles are characterized by a periodical structure.

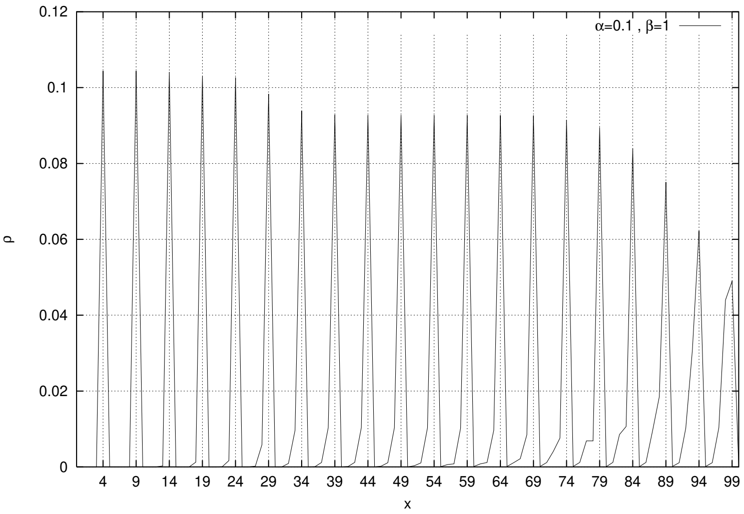

Figure 8.17: Density profile for a system with $\beta = 1$ and $\alpha = 0.1$ and bins length of 1. Cars travel with the average velocity of $v_{max} - \frac{a}{2}$. There are maximums each 5 steps.

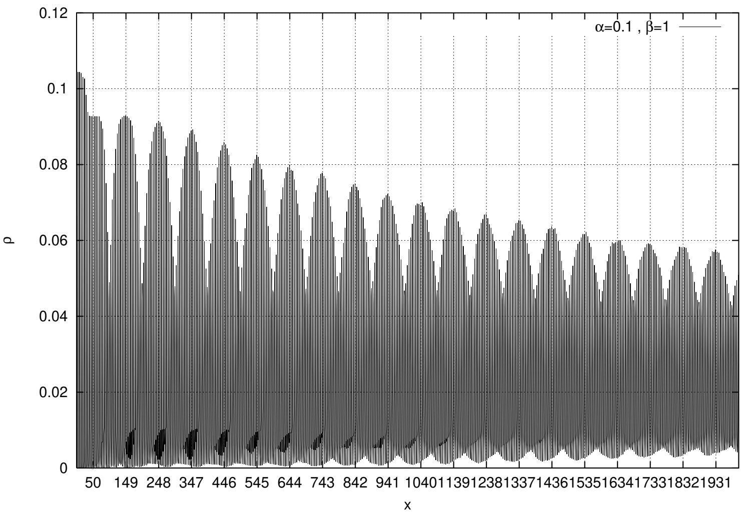

Figure 8.18: Period of oscillations for a system with a=0.1. The maximums are each 99 steps starting on 50.

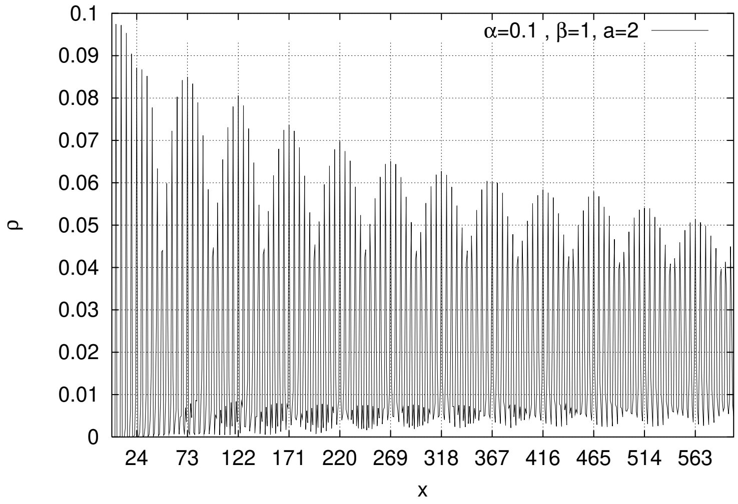

Figure 8.19: Period of oscillations for a system with a=0.2. The maximums are each 49 steps starting on 24.

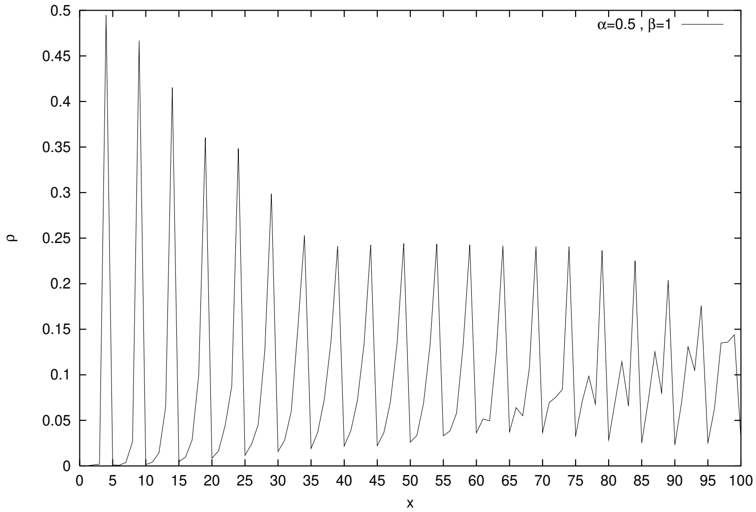

Figure 8.20: The probability of finding cars on different positions for systems with low interactions.

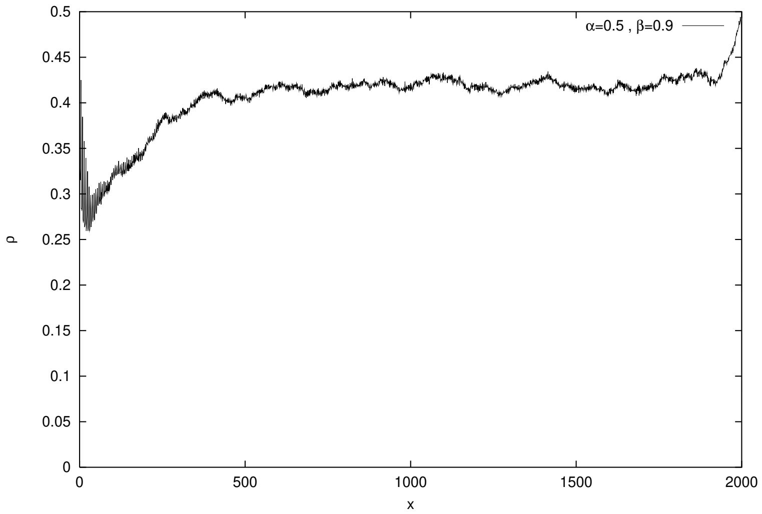

Figure 8.21: The probability of finding cars on different positions for interacting systems.

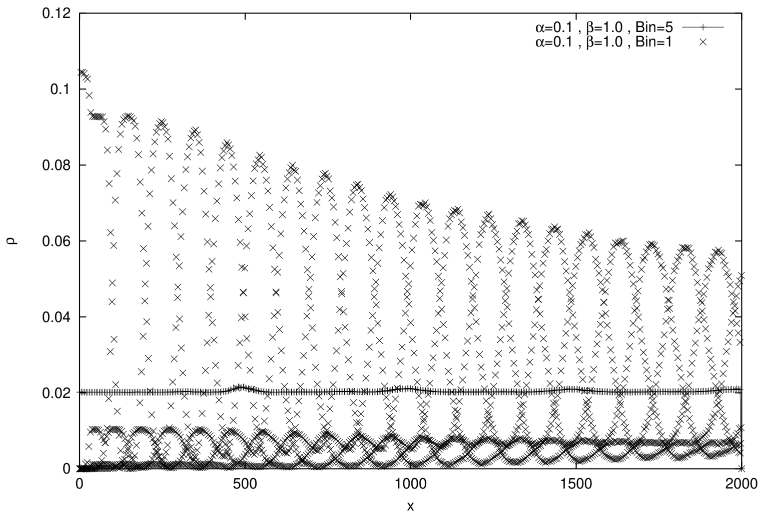

Figure 8.22: The density profile with different Bin-lengths

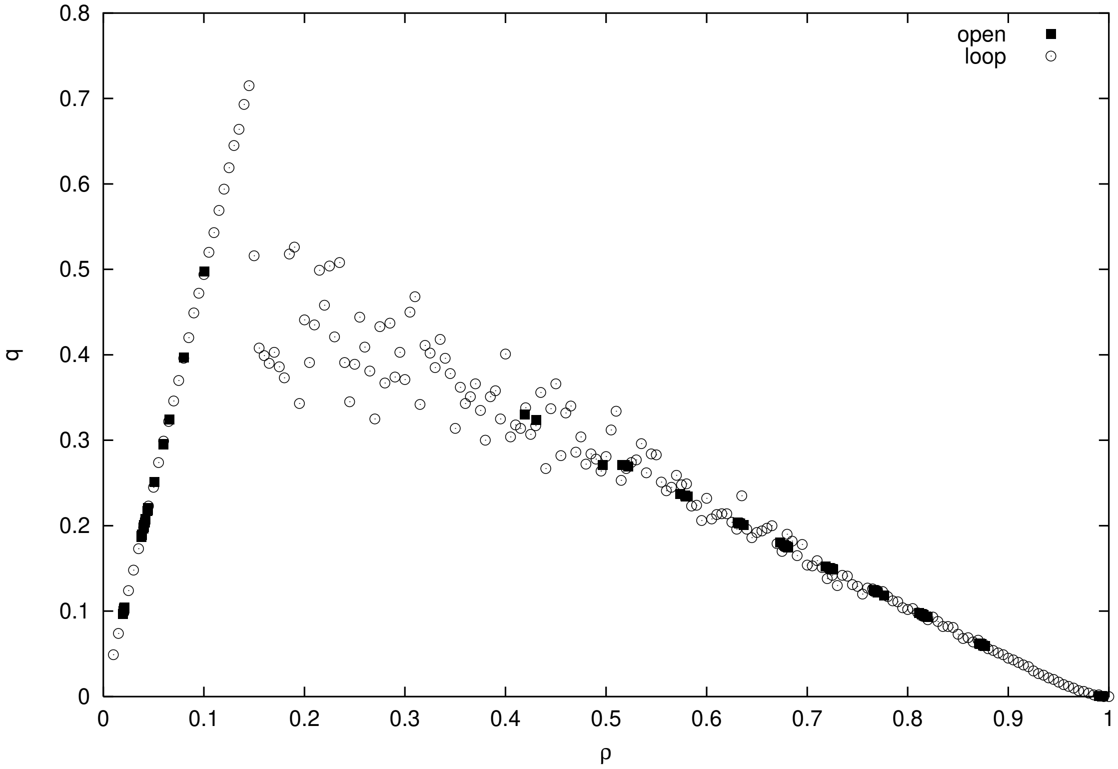

Figure 8.23: FD for the SK-model with periodical boundaries (empty circles). the balck points are coming from density profiles of the same system with open boundary conditions.

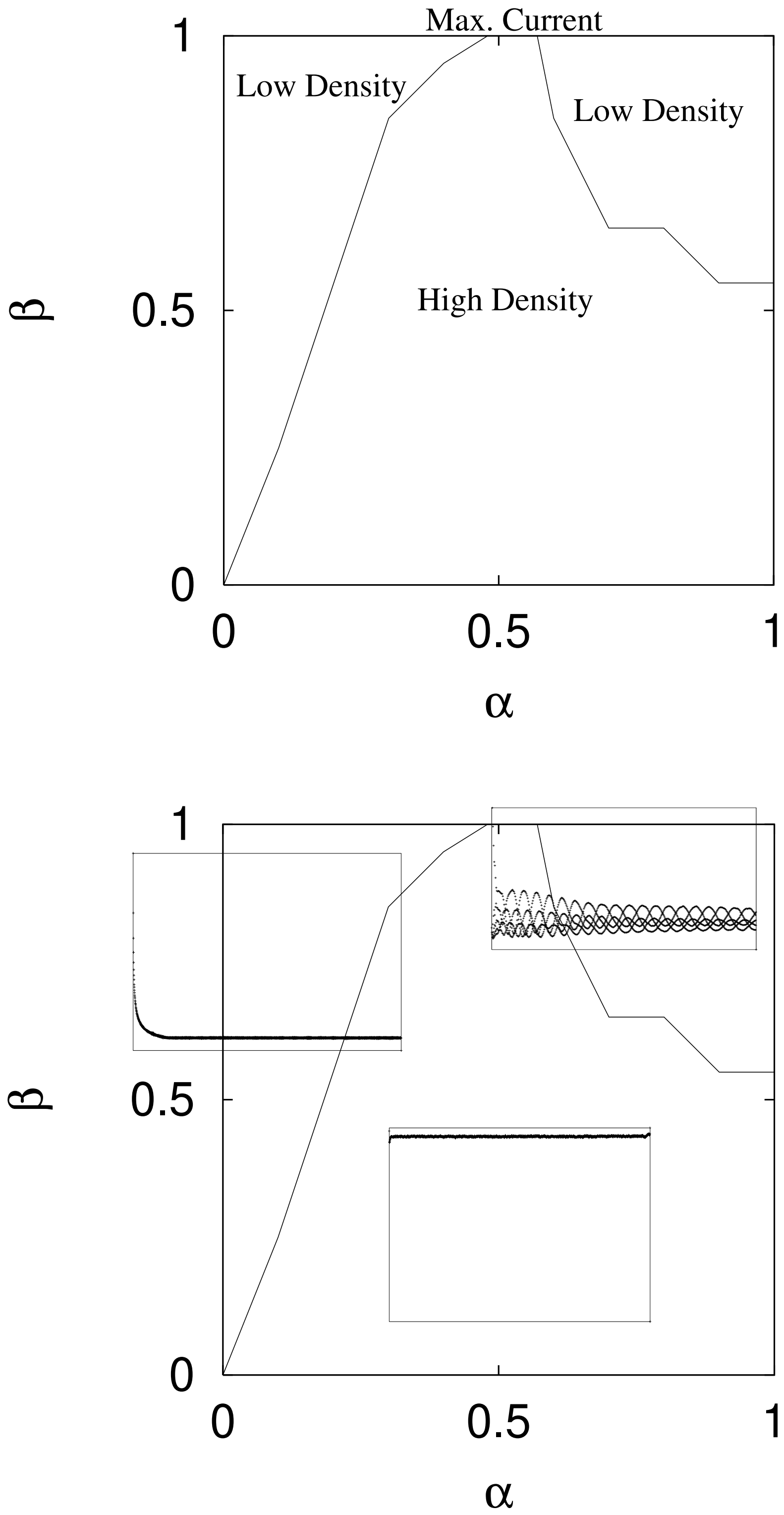

Figure 8.24: Phase diagram for the SK-model with open boundary conditions and an α oriented injecting strategy. Different phases, phase transition regions and the typical density profiles for each phase are shown. The maximum current phase with the *current* about 0.5 has been observed for system with open right boundary ($\beta = 1$) and injection rate between $\alpha = 0.48$ and $\alpha = 0.57$.

Chapter 9

High velocity oriented injection rule

As seen in the last section it is not easy to define left boundary conditions that allow the system to reach states that belong to the metastable branch and ensure safe movement of the injected car under any circumstances. The clue to find a strategy also to get these states is to have a closer look at the metastable regime on the corresponding periodic system [84].

While for the high density branch of the system on the loop on finds a bimodal distribution of the gaps between cars (see figure 5.3) in the high flow regime on the metastable branch this distribution is unimodal. The cars are flowing almost with v_{max}.

Instead of readjusting the initial speed v_{init} to achieve safety whenever there is one l_{car} place in front of the system [1] one can try to mimic that high ordered state.

To do so we try to inject cars with initial velocity of v_{max}. To guarantee a system free of crashes, we have to introduce a minimum safety gap_{init} to the preceding car.Choosing this gap similar to the gap on finds in the metastable regime, the injected car will stay collision free when updated according to the SK-model rules.

Using this strategy in spite of injection permission from α, no car will be injected for several time steps because of the lack of enough free space (gap_{init}) at the beginning of the system. This leads to the fact that there is a maximal density $\frac{1}{gap_{init}+1}$ one can reach at the left boundary.

For choosing the gap_{init} three criteria are formulated:

i) The gap_{init} should leave the system crash free.

ii) High currents should be reached (compared to the currents one finds in the metastable regime of the periodic system).

iii) The gap_{init} should be a minimum value from the set of all *gap*s that fulfill the criterion *i* and *ii*.

[1] Depending moreover on the inflow rate α

The last criterion increases the maximum reachable density at the system's entry and a bigger range of border densities can be investigated.

To find an appropriate value for the initial gap, we made several simulations with different values for gap_{init} , and measured the *current* for $\beta = 1$ to find a set of values which meet the criterion *ii*. Then we made some simulations with this set and tried to observe crashes in the system to filter out bad values. This could be done at best using $\beta \approx 0$. Then we chose the minimum value of the remaining values.

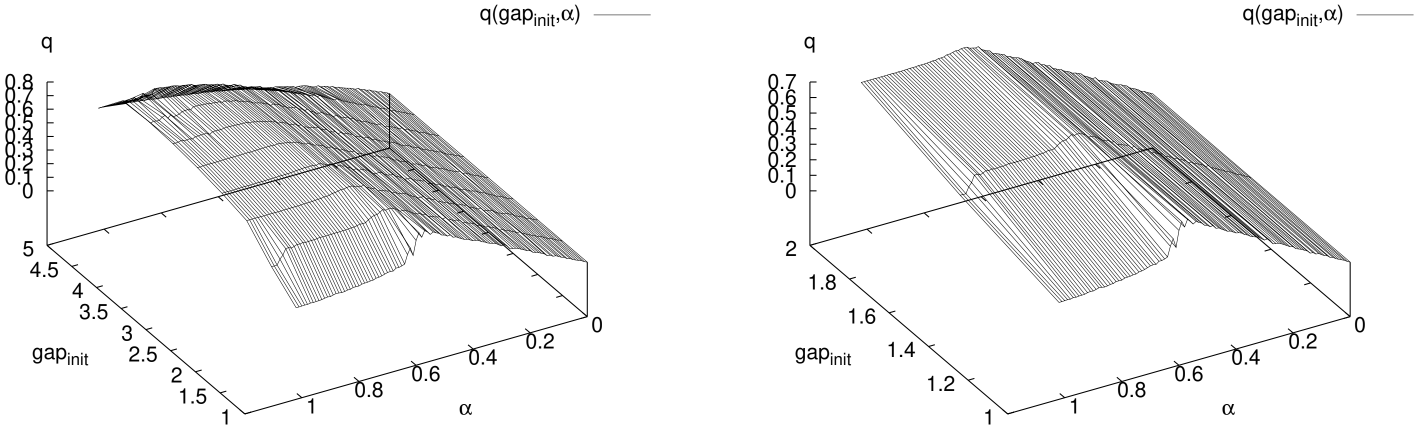

Figure 9.1: The relation between the *current*, α and $gap_{init} \in [1, 5]$ for $\beta = 1$. The *current* increases as α increases and either reaches a constant value or decreases and then reaches a constant value, depending on gap_{init}. For $5 > gap_{init} \geq 2$ the *current* reaches a constant value greater than 0.6, which is in the metastable region of a system with periodical boundary conditions. For $gap_{init} \geq 5$ the *current* decreases.

In figures. 9.1 (A,B) the relation between the *current*, α and gap_{init} for $\beta = 1$ is shown. The *current* increases as α increases and either reaches a constant value or decreases and then reaches a constant value, depending on gap_{init}. For $5 > gap_{init} \geq 2$ the *current* reaches a constant value greater than 0.6, which is in the metastable region of a system with periodical boundary conditions. For $gap_{init} \geq 5$ the *current* decreases drastically. This is obvious, it will be impossible to reach a density in the regime of maximum *current* if one waits for 5 free places before injecting a car in the system. The maximum *current* will be reached for a system with $\beta = 1$ and density of 0.15. For a system with $gap_{init} \geq 5$ the maximum reachable mean density is 0.1 (see chapter 5).

In Fig. 9.2 we have shown the the relation between the *current* and α for several values of gap_{init} for $\beta = 1$.

In simulations for systems with $\beta = 1$ we have observed crashes for $gap_{init} < 2$. We also observed crashes for systems with $\beta = 0$ for $gap_{init} < 2$. Also the only values of gap_{init} meeting the criterion *i*, *ii* are values $5 > gap_{init} \geq 2$. Because of the criteria *iii* we decided to work with $gap_{init} = 2$.

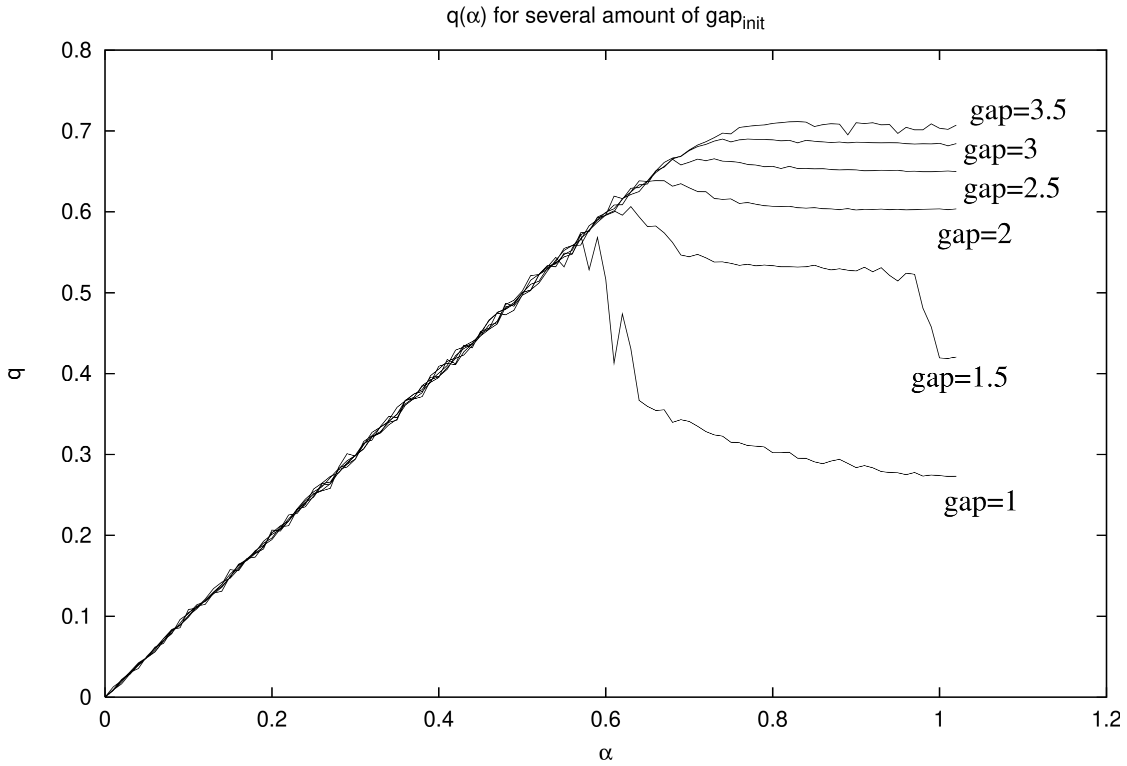

Figure 9.2: The relation between the *current* and α for several gap_{init} values $\in [1, 3.5]$. (See Fig. 9.1)

In the following chapter (9.1) we present the results of the simulations we have made with this injection rule.

9.1 Results for $gap_{init} = 2$

9.1.1 The fundamental diagram

The fundamental diagram measured for this system is very similar to the system with periodical boundary conditions. There is no hole in this fundamental diagram, since this role allows to reach the states on the metastable branch. It is actually the same difference, we had between α-*current* relations between both systems. With this injecting strategy, increasing α does not cause the decrease of the *current* in the way we saw in Chapter 8 In this diagram the maximum *current* and the metastable state would be reachable for systems with $\beta = 1.0$ (see chapter 9.1.2) .

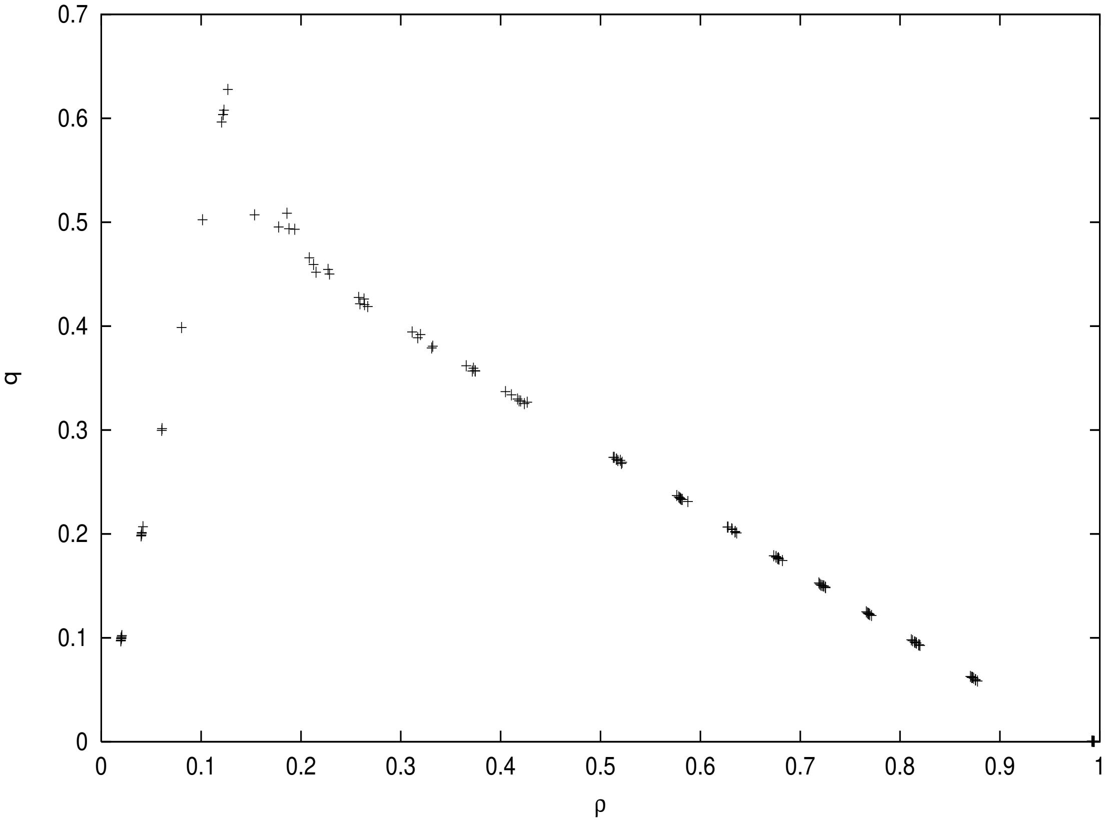

Figure 9.3: Fundamental diagram of the system with open boundaries. The maximum *current* and the metastable state are reached for systems with $\beta = 1.0$. The FD is similar to the FD of the system with periodical boundary conditions (see chapter 5).

9.1.2 Relations between α, β and the *current*, average velocity and the density

In this section we give an overview of the dependence of the current, average velocity and the density, measured in the middle of the system, on α and β.

In Figures 9.4 (A,B) we have shown the relation between the *current*, α and β from two different view angles. The *current* decreases strongly for the β values smaller than 1. The contours are the lines of the constant *current*.

In Figures 9.5 (A,B) we have shown the dependence of the density on α and β from two different view angles. The density used here is measured in the middle of the system in stationary state, which is the density of the plateau for systems in a certain phase. The contours could be interpreted as a phase transition line between high and low density phases.

In Fig. 9.6 we have shown the dependence of the average velocity on α and β. The average velocity gives us information about the state of the bulk in the system. The contours could be interpreted as a phase transition region between free flow and jamming phases.

9.1.3 Phase transitions and the phase diagram

Using the density profiles for systems with α's and β's between (0, 1) each 0.1 increments, we have drawn a phase diagram in Fig 9.7. Different phases are shown. The maximum current phase has been observed for systems with open right boundary (β = 1).

This phase diagram is similar to the phase diagram of the driven lattice gas with open boundary conditions discussed in section 6.3. The only difference is that in our model there exists a maximum current phase not depending on the size of the system. This might be an effect resulting from the different injection rule. The rule used here prepares high ordered cluster free states at the left boundary, similar to the meta stable states one finds in the periodic system.

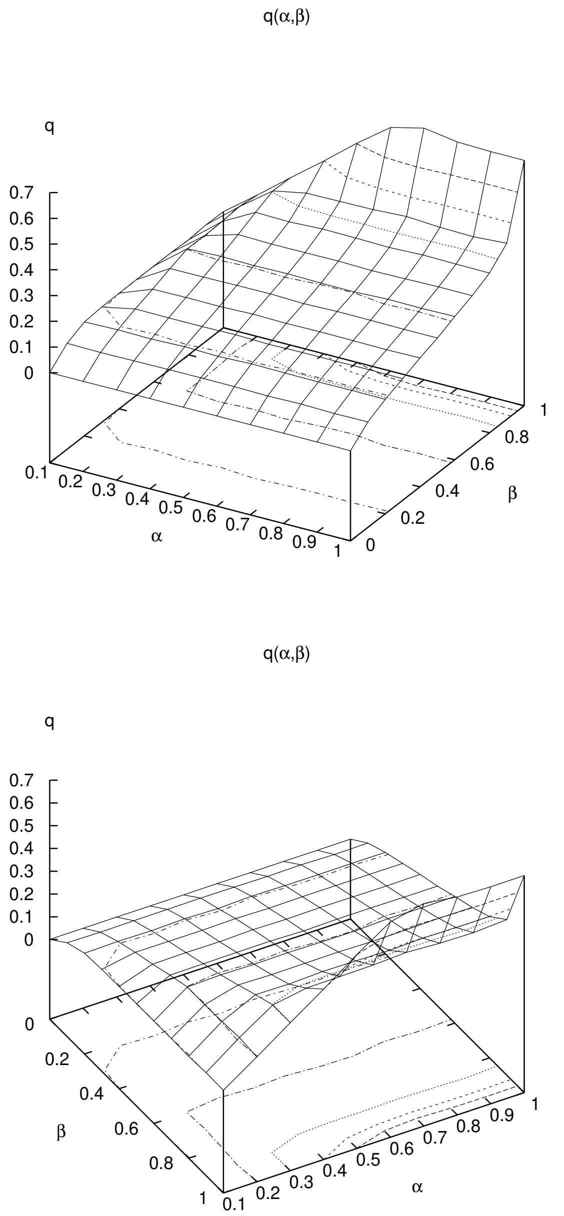

Figure 9.4: The relation between the *current*, α and β. (gap_{init} = 2). There is no decrease of *current* with increasing α anymore.

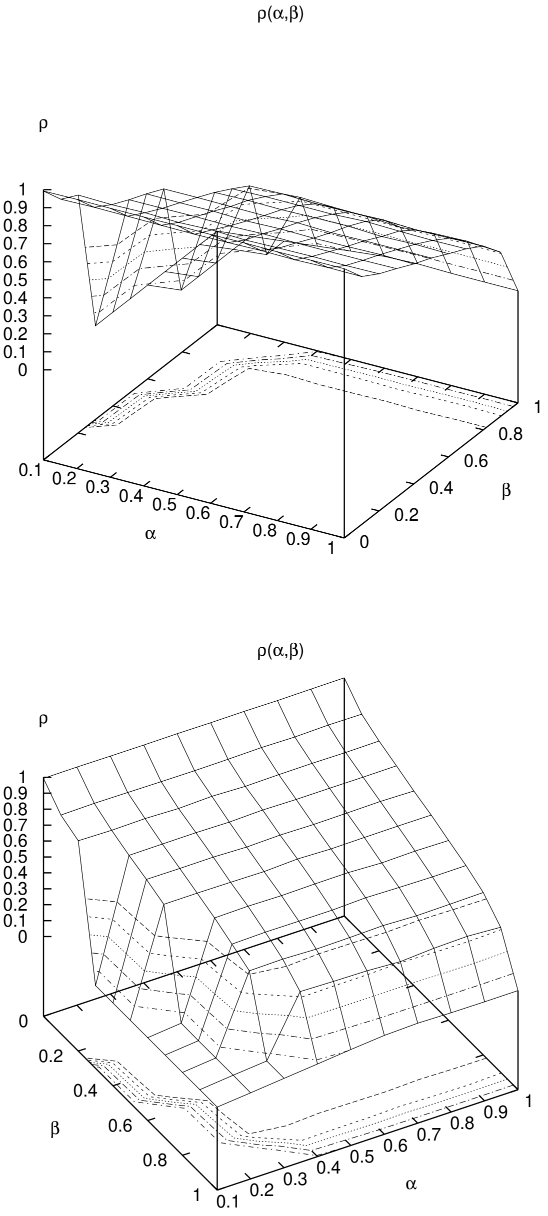

Figure 9.5: The relation between the density (measured in the middle of the system in stationary state), α and β (gap_{init} = 2). The contours could be interpreted as a phase transition line between high and low density phases.

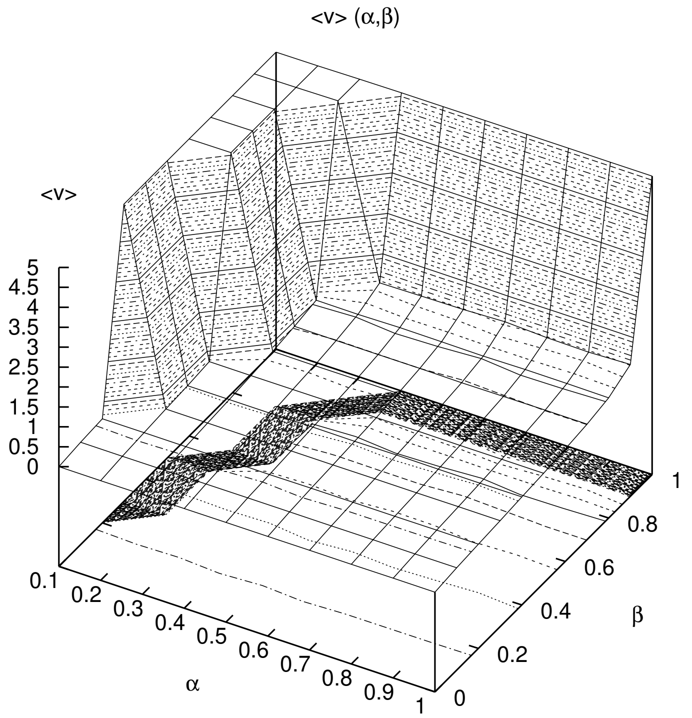

Figure 9.6: The relation between the average velocity, α and β (gap_{init} = 2). The contours could be interpreted as a phase transition region between free flow and jamming phases.

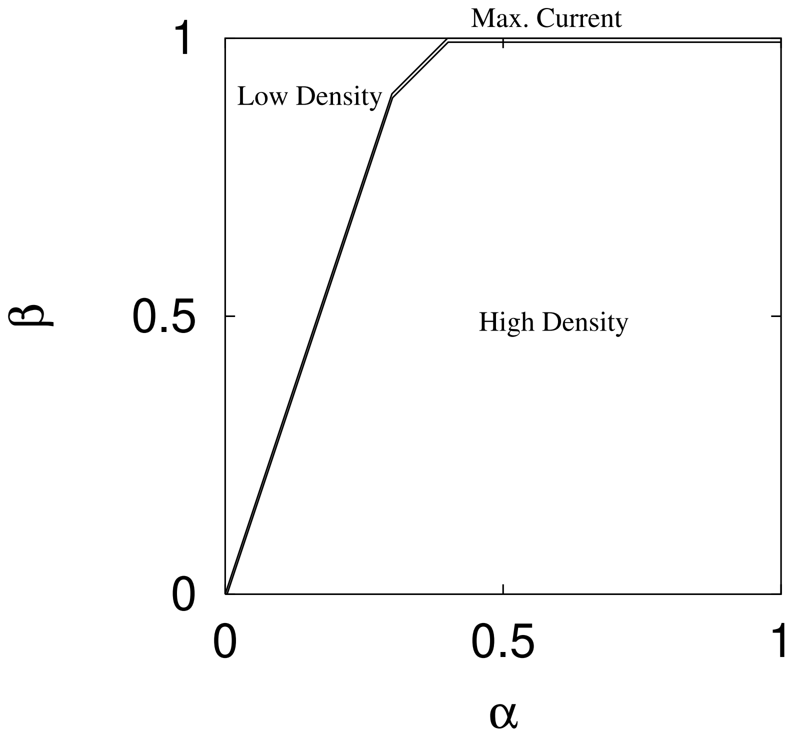

Figure 9.7: Phase diagram of the SK-model with open boundary conditions and maximum velocity oriented injecting rule. Different phases are shown. The maximum current phase has been observed for systems with open right boundary ($\beta = 1$).

Chapter 10

Summary, conclusion and outlook

The model introduced by Krauss et al. [1, 29] is a stochastic, collision-free model for traffic flow, which is continuous in space and discrete in time with bounded acceleration and deceleration rates. In a certain range of parameters this model (SK-model) shows metastable states of high flow. This fact is in agreement with empirical observations (chapter 2). Under periodical boundary conditions the model is well understood. It remains free of crashes, if the system has a collision-free initial configurations (chapter 5).

In this work we have studied the behavior of the SK-model with open boundary conditions. In contrast to periodic systems there are two tuning parameters, the injection rate α and the extraction rate β, that determine the system's bulk behavior. While there are already known results for open systems and discrete Nagel–Schreckenberg–type models (chapter 4), less is known for models that exhibit metastability. So we focused on the presence of these metastable states with high currents one knows from periodic systems.

To guarantee that the system remains free of crashes, one has to find a strategy to inject cars into the system. Two main methods solving this problem were discussed. First, one can determine an initial velocity to inject cars as a function of system parameters and state, which guarantees a crash-less travel of this cars at any time step (chapter 8). Second, one can fix a minimum free space at the beginning of the system (gap_{init}) and inject cars with a constant velocity (chapter 9).

The first injection strategy provides a car-injection-rate that keeps the density at the systems entry close to α. But the *current* through the system will decrease with increasing α, which causes an unusual phase diagram. The phase diagram of a system with the second injection rule looks very similar to those from other known systems. We found for the latter strategy that the system remains free of crashes for all values $gap_{init} \geq 2$, if cars are going to be injected with the velocity $v_{max} = 5$.

In general, interacting systems with open boundary conditions show *boundary induced phase transitions*. One distinguishes between three different phases, examining the functional dependence of the current through the system on the system parameters. These are the low-density, the high-density and the maximum current phase. All these phases are observed in the SK-model with open boundary conditions.

In order to explore the detailed structure of the phase diagram for the SK-model we used mainly numerical methods. To be more specific, we have used the fundamental diagram of the periodic system and the density profiles of the system with open boundaries conditions to analyze its different phases.

We have shown that the phases we found for the SK-model with open boundary conditions are comparable with those of the asymmetric simple exclusion process (ASEP). The ASEP is the simplest prototype model of interacting systems driven far from equilibrium. It is a generic model for the study of driven systems and boundary induced phase transitions [24, 79], [68]. Additional we found that our results are in agreement with the results recently done for a driven lattice gas that exhibits metastability (see section 6.3. Moreover, we have examined the extremal principle [83, 7] (see section 6.2) taking some examples of our simulations. For these examples we found that the phase diagram of the SK-model with open boundary conditions can indeed be described by using the left and right boundary densities and the fundamental diagram of the periodic system.

The implementation of right boundary conditions at the exit of the system without leaving the frame of the SK-model is still an open problem. Like in the ASEP, we let the cars leave the system with the extraction rate β. This means, we inserted a "block" with probability $1 - \beta$ at the end of the system to force the cars to stay in the system. This causes the cars to have a deceleration rate larger than the maximum deceleration rate introduced in the SK-model. Therefore flows belonging to the metastable regime of the model could only be observed for complete open system, i.e. $\beta = 1$.

More work should deal with the accurate determination of the correlation lengths for the description of the phase transitions. One of the problems finding the correlation lengths in SK-model with open boundaries is the oscillations in the density profiles (see chapter 8).

To define a method that is not depending on the specific implementation of the in/outflow rules one should reexamine the complete phases diagram of the model depending on the densities that result at the boundaries according to these rules. Doing this, further work should focus on other implementations of the right boundary rules to avoid such strong perturbation as we got using a "block" at the exit of the system.

Bibliography

[1] S. Krauss,(1998). Microscopic modeling of traffic flow. PhD thesis. ZAIK, University of Cologne.

[2] D. Chowdhury, L. Santen and A. Schadschneider in: *Statistical Physics of Vehicular Traffic and Some Related Systems*; Phys. Rep. **329**, 199 (2000)

[3] D.E. Wolf, M. Schreckenberg and A. Bachem (eds.), *Traffic and Granular Flow* (World Scientific, Singapore, 1996)

[4] M. Schreckenberg and D.E. Wolf (eds.), *Traffic and Granular Flow '97* (Springer, Singapore, 1998)

[5] R. Herman and K. Gardels, Sci. Am. **209**(6), 35 (1963)

[6] D.C. Gazis, Science, **157**, 273 (1967)

[7] A.B. Kolomeisky, G. Schütz, E.B. Kolomeisky and J.P. Straley, J. Phys. A **31**, 6911 (1998)

[8] I. Prigogine and R. Herman, *Kinetic Theory of Vehicular Traffic* (Elsevier, Amsterdam, 1971)

[9] K. Nagel, J. Esser and M. Rickert, in: Annu. Rev. Comp. Phys., ed. D. Stauffer (World Scientific, 1999)

[10] D. Helbing, *Verkehrsdynamik: Neue Physikalische Modellierungskonzepte* (in German) (Springer, 1997)

[11] B.D. Greenshields, Proc. Highw. Res. **14**, 448 (1935)

[12] A.D. May, *Traffic Flow Fundamentals* (Prentice-Hall, 1990)

[13] Th. Winzer, *Messung von Beschleunigungsverteilungen (Measurements of Acceleration Distributions)*, Forschung Straßenbau und Straßentechnik (Research in Road Construction and Traffic Engineering), Federal Ministry of Transportation, Bonn, Germany (1980)

[14] M. Bando, K. Hasebe, A. Nakayama, A. Shibata, and Y. Sugiyama, Structure Stability of Congestion in Traffic Dynamics, Japan J. Indust. Appl. Math.**11**(2), 203–223 (1994)

[15] B.S. Kerner, and P. Konhäuser, Cluster effect in initially homogeneous traffic flow. Jrn Phys. Rev. E **48**(4), R 2335 (1993)

[16] S. Yukawa, M. Kikuchi, Density Fluctuations in Traffic Flow, Jrn. Phys. Soc. Jap. **65**(4) 916-919, (1996)

[17] M. Cremer, J. Ludwig, A Fast Simulation Model for Traffic Flow on the Basis of Boolean Operations, Jrn Mathematics and Computers in Simulation **28**, 297–303 (1986)

[18] A. Bachem, K. Nagel, M. Rickert, Ultraschnelle mikroskopische Verkehrssimulationen, Jrn Parallele Datenverarbeitung aktuell TAT, R. Flieger and R. Greb ed. (1994)

[19] Ch.L. Barret, S. Eubank, K. Nagel, S. Rasmussen, J.Riodan, and M. Wolinsky, Issues in the Representation of traffic using Multi–Resolution Cellular Automata, Los Alamos National Laboratory Technical Report: LA/UR 95–2658 (1995)

[20] R.D. Kühne, in Jrn Proceedings of the Ninth International Symposium on Transportation and Traffic Theory, edited by I. Volmuller and R. Hamerslag (VNU Science, Utrecht, 1984)

[21] D. Helbing, Improved fluid-dynamic model for vehicular traffic, Jrn Phys. Rev. E **51**, 3164–3169 (1995).

[22] C. Appert and L. Santen. Boundary induced phase transitions in driven lattice gases with meta stable states. 2000. arXiv:cond-mat/0004048

[23] R. Barlovic, L. Santen, A. Schadschneider, M. Schreckenberg, Metastable States in CA models for Traffic Flow. Jrn cond-mat/9711282 (1997)

[24] B. Schmittmann and R.K.P. Zia, in: *Phase Transitions and Critical Phenomena*, Vol. 17, eds. C. Domb and J.L. Lebowitz (Academic Press, 1995); Phys. Rep. **301**, 45 (1998); R.K.P. Zia, L.B. Shaw, B. Schmittmann and R.J. Astalos, `cond-mat/9906376`

[25] H. Spohn, *Large Scale Dynamics of Interacting Particles* (Springer, 1991)

[26] V. Privman (ed.), *Nonequilibrium Statistical Mechanics in One Dimension* (Cambridge University Press, 1997)

[27] J.T. MacDonald, J.H. Gibbs and A.C. Pipkin, Biopolymers **6**, 1 (1968); J.T. MacDonald and J.H. Gibbs, Biopolymers **7**, 707 (1969)

[28] K. Nagel and M. Schreckenberg, J. Physique I, **2**, 2221 (1992); K. Nagel, in: *Physics Computing '92*, eds. R.A. de Groot and J. Nadrchal (World Scientific, 1993), p.419; K. Nagel, *High Speed Microsimulations of Traffic Flow*, Ph.D Thesis, University of Cologne (1995).

[29] S. Krauss, P. Wagner and C. Gawron, Phys. Rev. E **54**, 3707 (1996); **55**, 5597 (1997)

[30] S. Krauss, in: [4], p. 269; see also S. Krauss, *Microscopic Modeling of Traffic Flow: Investigation of Collision Free Vehicle Dynamics*, DLR-Forschungsbericht 98-08

[31] H. Greenberg, Op. Res. **7**, 79 (1959)

[32] F.L. Hall, in [3], p. 11

[33] F.L. Hall, B.L. Allen and M.A. Gunter, Transp. Res. **A20**, 197 (1986)

[34] L. Neubert, L. Santen, A. Schadschneider and M. Schreckenberg, Phys. Rev. E **60**, 6480 (1999)

[35] D H. Hoefs, *Untersuchung des Fahrverhaltens in Fahrzeugkolonnen*, Straßenbau und Verkehrstechnik, Heft 8, Federal Ministry of Transportation, Bonn, Germany (1972)

[36] C.F. Daganzo, M.J. Cassidy, R.L. Bertini, Transp. Res. A **33**, 365 (1999)

[37] J. Treiterer: Ohio State Technical Report No. PB 246 094, (1975)

[38] B.S. Kerner and H. Rehborn, Phys. Rev. E **53**, R1297 (1996)

[39] B.S. Kerner and H. Rehborn, Phys. Rev. E **53**, R4275 (1996)

[40] B.S. Kerner, in [4], p. 239

[41] L.A. Pipes, An operational analysis of traffic dynamics. J. Appl. Phys. vol 24, 274 (1953)

[42] M. Bando, K. Hasebe, A. Nakayama, A. Shibata, and. Y. Sugiyama, Dynamical model of traffic congestion and numerical simulation, Phys. Rev. E **51**(2), 1035–1042 (1995).

[43] B.S. Kerner, Traffic flow: Experiment and Theory, Paper presented at *Traffic and Granular Flow*, Duisburg, Germany (1997)

[44] S. Yukawa, M. Kikuchi, Coupled–Map Modeling of One–Dimensional Traffic Flow. Jrn. Phys. Soc. Jap. **64**(1) 33-38, (1995)

[45] P.G. Gipps, A behavioural car following model for computer simulation, Transpn. Res. B, vol 15B, 105–111 (1981)

[46] H. Schütt, book Entwicklung und Erprobung eines sehr schnellen, bitorientierten Verkehrssimulationssystems für Straßennetze, Schriftenreihe der AG Automatisierungstechnik, TU Hamburg Harburg (1991)

[47] K. Nagel, and M. Paczuski. Emergent traffic jams Phys. Rev. E, vol 51, 2909 (1995).

[48] K. Nagel, and M. Schreckenberg. A cellular automaton model for freeway traffic. *J. Physique I*, 2:2221 (1992).

[49] K. Nagel, High Speed Microsimulations of Traffic Flow, Doctoral dissertation, University of Cologne (1995)

[50] A. Schadschneider, and M. Schreckenberg. Cellular automaton models and traffic flow. *Journal of Physics A*, 26, L679 (1993).

[51] M. Schreckenberg, A. Schadschneider, K. Nagel, and N. Ito, Discrete stochastic models for traffic flow, Phys. Rev. E vol 51, 2939 (1995).

[52] H. Emmerich, E. Rank, Investigating traffic flow in the presence of hindrances by cellular automata, Physica A vol 216, 435–444 (1995)

[53] H. Emmerich, Simulation im Straßenverkehr, Dissertation, Universität Dortmund, Fakultät für Bauwesen (1997)

[54] H. Emmerich, E. Rank, An improved cellular automaton model for traffic flow simulation, Physica A vol 234, 676–686 (1997)

[55] S. Krauß, P. Wagner, and C. Gawron Continuous Limit of the Nagel–Schreckenberg–Model, Phys. Rev. E., vol 54 ,3707 (1996)

[56] M.J. Lighthill, G.B. Whitham, On kinematic waves II: A theory of traffic flow on long crowded roads, Proc. R. Soc. London **A229**, 317–345 (1955)

[57] C.F. Daganzo, The Cell Transmission Model: A dynamic Representation of Highway Traffic Consistent with the Hydrodynamic Theory, Transpn. Res. B **28B** 269–287 (1994)

[58] C.F. Daganzo, The Cell Transmission Model, Part II Network Traffic Transpn. Res. B **29B** 79–93 (1995)

[59] C.F. Daganzo, Requiem for second order fluid approximations of traffic flow, Transpn. Res. B **29B)**, 277–286 (1995)

[60] G.F. Newell, A simplified theory of kinematic waves in highway traffic, Part I: General Theory Transpn. Res. B. **27B**(4), 281-287 (1993)

[61] G.F. Newell, A simplified theory of kinematic waves in highway traffic, Part II: queueing at freeway bottlenecks Transpn. Res. B. **27B**(4), 289–303 (1993)

[62] G.F. Newell, A simplified theory of kinematic waves in highway traffic, Part III: Multi–destination flows Transpn. Res. B. **27B**(4), 290–314 (1993)

[63] R.E. Franklin, On the flow–concentration relationship for traffic, in Proc. 2nd Int. Symp. Theory Road Traffic Flow, 120–128, London 1963

[64] P. Ross, Traffic dynamics. Transpn. Res. vol 22B, 421-436 (1988)

[65] R.D. Kühne, Transp. Res. Rec. vol 1320, 251 (1991)

[66] M. Schreckenberg, A. Schadschneider, K. Nagel, and N. Ito, *Phys. Rev. E* **51**, 2939 (1995).

[67] A.Schadschneider and M. Schreckenberg, *J. Phys. A* **26**, L679 (1993).

[68] A.Schadschneider, *Eur. Phys. J. B* **10**, 573 (1999).

[69] R.D. Kühne, Traffic Patterns in unstable traffic flow on freeways, book Highway Capacity an Level of Service, Brannolte (ed.), Balkema, Rotterdam (1991)

[70] B.S. Kerner, and P. Konhäuser, Structures and parameters of clusters in traffic flow. Phys. Rev. E **50**, 54 (1994).

[71] M. Cremer, Der Verkehrsfluß auf Schnellstraßen. Heidelberg, Germany: Springer Verlag (1979)

[72] M. Hilliges, Ein phänomenologisches Modell des dynamischen Verkehrsflusses in Schnellstraßennetzen, Dissertation, Universität Stuttgart (1995)

[73] I. Prigogine, R. Herman, Kinetic theory of vehicular traffic, American Elsevier Publishing Comp. Inc., NewYork (1971)

[74] S. Wolfram, *Theory and Applications of Cellular Automata*, (World Scientific, 1986); *Cellular Automata and Complexity* (Addison-Wesley, 1994).

[75] R. Barlovic, L. Santen, A. Schadschneider and M. Schreckenberg, Eur. Phys. J. B **5**, 793 (1998)

[76] B.S. Kerner, and P. Konhäuser, Structures and parameters of clusters in traffic flow. Phys. Rev. E **50**, 54 (1994).

[77] A. Schadschneider, and M. Schreckenberg, Traffic flow models with 'slow-to-start' rules. Ann. Physik **6**, 541 (1997)

[78] M. Fukui, Y. Ishibashi, Traffic Flow in 1D Cellular Automaton Model Including Cars Moving with High Speed. J. Phys. Soc. Jp. **65**(6) 1868 – 1870 (1996)

[79] G. Schütz, in: *Phase Transitions and Critical Phenomena*, eds. C. Domb and J.L. Lebowitz (to appear)

[80] G. Schütz and E. Domany, J. Stat. Phys.**72**, 277 (1993)

[81] N. Rajewsky, L. Santen, A. Schadschneider and M. Schreckenberg, J. Stat. Phys. **92**, 151 (1998)

[82] J. de Gier and B. Nienhuis, Phys. Rev. E **59**, 4899 (1999)

[83] V. Popkov and G. Schütz, Europhys. Lett. **48**, 257 (1999)

[84] Nils Eissfeldt, private communication.

Deutsche Zusammenfassung

Von Krauss [1],[30] wurde eine räumlich kontinuierliche Erweiterung des Nagel-Schreckenberg-Modells vorgestellt. Der Modellentwicklung (SK-Modell) gingen Untersuchungen über das Verhalten des kontinuierlichen Limes des Nagel-Schreckenberg-Modells [28] und den Zusammenhang von begrenztem Bremsvermögen und der Existenz metastabiler Zustände voraus.

Das SK-Modell mit periodischen Randbedingungen ist gut untersucht und verstanden. Diese Arbeit beschäftigt sich mit den Eigenschaften des SK-Modells unter offenen Rändern. Zum einen entspricht dies der Situation, die man in der Realität vorfindet (z.B. Auffahrten auf Autobahnen). Zum anderen zeigen eindimensionale Nichtgleichgewichtssysteme randinduzierte Phasenübergänge. Solche wurden bislang hauptsächlich an Systemen ohne metastabile Zustände untersucht.

Ein grosses Problem im Rahmen eines kontinuierlichen Modells ist die Definition passender Ein- und Ausfütterregeln. Die Probleme, die hierbei auftreten, werden ausführlich diskutiert und klassifiert. Aus der Diskussion werden zwei unterschiedliche Regelsätze abgeleitet, mit deren Hilfe sich die Eigenschaften des Modells und seiner Phasen untersucht lassen. Die Ergebnisse zeigen, daß die auftretenden Phasen in stärkerem Masse von den realisierten Regeln an den Systemrändern abhängen als in diskreten Modellen.

Die Ergebnisse und Phasen des offenen Systems werden in Zusammenhang zu den Eigenschaften des periodischen Systems gebracht. Darüber hinaus werden sie eingeordnet in Ergebnisse aus Arbeiten zum Asymmetrischen Einfachen Exklusionsprozess (ASEP), einem einfachen diskreten Vertreter eindimensionaler Nichtgleichgewichtssysteme. Die Ergebnisse passen gut zu dem dort abgeleiteten allgemeinen Zusammenhang zwischen dem Fundamentaldiagramm des periodischen Systems und den anzutreffenden Phasen im korrespondierenden offenen System.

Desweiteren werden Methoden vorgestellt, um das Phasendiagramm zu bestimmen. Von besonderem Interesse ist hierbei das stationäre Dichteprofil. Es konnte ein Erklärung für die starken Oszillationen geliefert werden, die man in ihnen in Phasen niedriger Dichte findet. Diese erschweren eine exakte Bestimmung der Dichten am Systemeingang. Mit Hilfe einer Betrachtung der Randdichten für ausgewählte Fälle konnte gezeigt werden, daß sich das Phasendiagramm des SK-Modells mit offenen Rändern mit Hilfe eines Extremalprinzipes für den Systemfluss (sehe Kapitel 6.2 und [83],[7])erklären lässt.

Danksagung

An dieser Stelle möchte ich Herrn Priv. Doz. Dr. Andreas Schadschneider und Herrn Nils Eissfeldt für die hervorragende Betreuung und die Hilfe bei der Korrektur des Manuskriptes danken. Herrn Prof. Dr. Ulrich Faigle danke ich für das Interesse an dieser Arbeit und die Zurverfügungstellung eines Arbeitsplatzes. Grossen Dank möchte ich auch Herrn Dr. Peter Wagner für viele konstruktive Vorschläge und Gespräche aussprechen.

Ich danke Julia Heygster und Pejman Kayvani, die mir bei meinem Zeitmangel sehr viel geholfen haben. Mein besonderer Dank gilt meinem Sohn, der mir viele Lebensfreude gegeben hat.

Erklärung

Ich versichere, daß ich dieser Arbeit selbstständig gemacht habe. Alle benutzten Hilfsmittel, Quellen und Zitate sind kenntlich gemacht worden.

Alireza Namazi, April 2001.